Thesis for the degree of doctor of philosophy

Low noise frequency combs and injection locking for broadly tunable laser sources and tomography

J. Connor Skehan

CHALMERS

Photonics Laboratory
Department of Microtechnology and Nanoscience - MC2
Chalmers University of Technology
Göteborg, Sweden, 2023

Low noise frequency combs and injection locking for broadly tunable laser sources and tomography
J. Connor Skehan
Göteborg, December 2023

Chalmers University of Technology
Microtechnology and Nanoscience - MC2
Photonics Laboratory
SE-412 96 Göteborg, Sweden
Phone: +46 (0) 31 772 1000

ISBN : 978-91-7905-964-4
Ny serie (ISSN0346-718X)
Löpnummer : 5430

Printed in Sweden by Reproservice, Chalmers University of Technology
Göteborg, Sweden, November 2023

Low noise frequency combs and injection locking for broadly tunable laser sources and tomography

J. Connor Skehan
Photonics Laboratory
Department of Microtechnology and Nanoscience - MC2
Chalmers University of Technology

Abstract

Lasers have revolutionized the world of physics by providing a highly coherent source of photons which may be used for a large variety of purposes. Here, we study the noise properties of frequency combs - a special class of frequency stabilized and mutually coherent multi-mode lasers, as well as the optical injection locking of comb tones as a means for low noise amplification and tone selection. A variety of applications are discussed, along with more fundamental properties of the systems in question. Particular focus is placed on the exceptionally low phase noise of these sources.

Several comb sources are investigated, including bulk electo-optic combs, on-chip anomalous dispersion micro-combs, and on-chip normal dispersion photonic molecules. Similarly, several sources are investigated for their use in optical injection locking, including DFB slave laser arrays, and multi-mode FP lasers. Noise mitigation is also investigated at length, with a focus on PID control loops and thermorefractive noise reduction at high temperature. Furthermore, significant attention is given to the noise analysis of frequency combs and optical injection locking. The mutual coherence of comb tones is investigated, along with the growth of noise as a function of comb mode index. Finally the role of injected noise is studied in the case of optical injection locking near the limit of stability for locking.

Keywords: optical frequency comb, optical injection locking, phase noise, laser noise, laser stabilization

Publications

This thesis is based on the work contained in the following papers :

[A] **J. Connor Skehan**, Corentin Naveau, Jochen Schröder, and Peter Andrekson
"Widely tunable, low linewidth, and high power laser source using an electro-optic comb and injection-locked slave laser array",
Optics Express, vol. 29, no. 11, May 2021

[B] **J. Connor Skehan**, Oskar B. Helgason, Jochen Schröder, Victor Torres-Company, and Peter Andrekson
"Widely tunable narrow linewidth laser source based on photonic molecule microcombs and optical injection locking",
Optics Express, vol. 30, no. 12, June 2022.

[C] **J. Connor Skehan**, Anamika Nair Karunakaran, Poul Varming, Óskar B. Helgason, Patrick B. Montague, Jochen Schröder, Minhao Pu, Kresten Yvind, Victor Torres-Company, and Peter A. Andrekson
"Thermorefractive noise reduction of photonic molecule frequency combs using an all-optical servo loop",
Optics Express, vol. 31, no. 21, October 2023.

[D] **J. Connor Skehan**, Magnus Karlsson, and Peter A. Andrekson
"Pre-amplified optical injection locking with low input power",
Submitted to *Optics Express*.

[E] Paul J. Marchand, Johann Riemensberger, **J. Connor Skehan**, Jia-Jung Ho, Martin H. P. Pfeiffer, Junqiu Liu, Christoph Hauger, Theo Lasser, Tobias J. Kippenberg
"Soliton microcomb based spectral domain optical coherence tomography",
Nature Communications, 12:427, 2021.

The following works represent the sum total of my other scientific work, excluding those previously mentioned (Papers [A-E]). The following list therefore represents all scientific publications in my name which are not included as part of this thesis, at the time of writing :

[F] **Connor Skehan**, Bin Ai, Steven R Larson, Keenan M Stone, William M Dennis, Yiping Zhao
"Plasmonic and SERS performances of compound nanohole arrays fabricated by shadow sphere lithography",
Nanotechnology, volume 29.9, 095301

[G] Mikhail Churaev, Simon Honl, Rui Ning Wang, Charles Mohl, Tianyi Liu, **J Connor Skehan**, Johann Riemensberger, Daniele Caimi, Junqiu Liu, Paul Seidler, Tobias J Kippenberg
"Hybrid Si3N4-LiNbO3 integrated platform for electro-optic conversion",
CLEO : Science and Innovations, May 2020, STh1F.3

[H] Jeff Chiles, Nima Nader, Eric J Stanton, Daniel Herman, Galan Moody, Jiangang Zhu, **J Connor Skehan**, Biswarup Guha, Abijith Kowligy, Juliet T Gopinath, Kartik Srinivasan, Scott A Diddams, Ian Coddington, Nathan R Newbury, Jeffrey M Shainline, Sae Woo Nam, Richard P Mirin
"Multifunctional integrated photonics in the mid-infrared with suspended AlGaAs on silicon",
Optica, Volume 6.9, 1246-1254

[I] Alexey Tikan, Johann Riemensberger, Kenichi Komagata, Simon Hönl, Mikhail Churaev, **Connor Skehan**, Hairun Guo, Rui Ning Wang, Junqiu Liu, Paul Seidler, Tobias J Kippenberg
"Emergent nonlinear phenomena in a driven dissipative photonic dimer",
Nature Physics, Volume 17.5, 604-610

[J] Hao Tian, Junqiu Liu, Bin Dong, **J Connor Skehan**, Michael Zervas, Tobias J Kippenberg, Sunil A Bhave
"Hybrid integrated photonics using bulk acoustic resonators",
Nature Communications, Volume 11.1, 1-8

[K] Hao Tian, Junqiu Liu, **Connor Skehan**, Anat Siddharth, Tobias J Kippenberg, Sunil A Bhave
"A nitride ring isolator",
CLEO : Science and Innovations, STu4O.2

[L] A Tikan, J Riemensberger, K Komagata, S Hönl, M Churaev, **C Skehan**, H Guo, RN Wang, J Liu, P Seidler, TJ Kippenberg
"Dissipative Kerr solitons in a photonic dimer",
2020 Conference on Lasers and Electro-Optics (CLEO)

Contents

Acknowledgements

I extend my enormous gratitude to the many people in my life who have helped me throughout the years. In particular, I offer my thanks to those people who instilled in me certain values and virtues which still serve me today. My love of learning, my passion for life, and my commitment to continuous self betterment didn't simply emerge from a vacuum. These values were taught to me by family, friends, educators, and the many role models I've met or learned from along the way, and for that I am eternally grateful. I would also like to extend my gratitude to those patrons who provided funding along the way. A special thanks is therefore in order to the Knut och Alice Wallenbergs Stiftelse and Vetenskapsrådet (VR-2015-00535).

J. Connor Skehan
Göteborg, November 2023

On the planet Earth, man had always assumed that he was more intelligent than dolphins because he had achieved so much - the wheel, New York, wars and so on - whilst all the dolphins had ever done was muck about in the water having a good time. But conversely, the dolphins had always believed they were far more intelligent than man - for precisely the same reasons.

Douglas Adams
The Hitchhiker's Guide to the Galaxy

Acronyms

AOM	acousto-optic modulator
ASE	amplified spontaneous emission
BPF	bandpass filter
CEO	carrier-envelope offset
CW	continuous wave
DFB	distributed feedback
DSP	digital signal processing
DUT	device under test
ECDL	external cavity diode laser
EDFA	erbium-doped fiber amplifier
EM	electro-magnetic
EO	electro-optic
ESA	electric spectrum analyzer
FBG	fiber Bragg grating
FP	Fabry-Perot
FSR	free spectral range
FT	Fourier transform
FWHM	full-width half-max
HNLF	highly nonlinear fiber
HPF	high pass filter
LIDAR	light detection and ranging
LLE	Lugiato-Lefever equation
LPF	low-pass filter
MI	modulation instability

MZI	Mach Zehnder interferometer
MZM	Mach Zehnder modulator
NLSE	nonlinear Schrödinger equation
NF	noise figure
OCT	optical coherence tomography
OFC	optical frequency comb
OIL	optical injection locking
OTDR	optical time domain reflectometry
P/FN	phase / frequency noise
PID	proportional, integral, and derivative
PSA	phase sensitive amplification
PSD	power spectral density
RF	radio frequency
RIN	relative intensity noise
RMS	root mean squared
SCG	supercontinuum generation
SMSR	side-mode suppression ratio
SNR	signal to noise ratio
SOA	semiconductor optical amplifier
SWaP	size, weight, and power

CHAPTER 1

Introduction

1.1 Personal Research Background

This thesis encompasses a selection of my work done in the years since my Master's degree, during which time I have been primarily interested in the noise properties of optical frequency comb (OFC)s [Papers A-C & E] and optical injection locking (OIL) [Papers A,B & D]. In this text, my work on frequency combs is focused on the intensity noise, phase and frequency noise, and mutual coherence of tones which originate from anomalous dispersion microresonator frequency combs, coupled cavity normal dispersion microresonator frequency combs, and electro-optic (EO) combs. Meanwhile, my work on optical injection locking focuses on the selection and amplification of these comb tones, as well as a detailed analysis of the noise properties of the final injection locked output, especially in the case of optical pre-amplification.

This work was done primarily at Chalmers University of Technology in Sweden, but also includes work done at École Polytechnique de Lausanne (EPFL) in Switzerland, and work done in Copenhagen in collaboration with the Technical University of Denmark (DTU) and NKT Photonics.

There is a significant body of research which has been published in my name since my Master's degree which is not included in this thesis. This includes my work on thin film lithium niobate electro-optic modulators

[Paper G], on hybrid structures for on-chip acousto-optic modulation [Papers J & K], and on anomalous dispersion coupled cavity systems [Papers I & L]. Moreover, published work done during my Bachelor's on noble metal compound nanohole arrays [Paper F] and during my Master's on AlGaAs nonlinear optics [Paper H] and time resolved dual comb spectroscopy are not included in this thesis.

1.2 Contents of the Thesis

The thesis begins with a brief introduction which aims to frame the reader's expectations. As such, it includes an overview of what is included in the thesis, provides historical context for my research, explains the scientific merit thereof, and provides a short overview of the future outlook of this work.

The second chapter then offers the reader a more detailed understanding of semiconductor lasers [1–5] and their noise properties, with a special focus on intensity noise, phase and frequency noise, and the mutual coherence of any two optical tones - as well as various methods to measure and control such devices.

Chapter three covers optical injection locking at length [6–11]. In particular, this chapter serves to extend the rate equation discussion of semiconductor lasers provided in the first chapter in order to better understand the impact of light which is externally injected into the laser cavity, and to provide a set of simplifications and approximations which will aide the reader later on.

The fourth chapter then discusses frequency combs [12, 13], a special case of mutual coherence in multi-mode lasers which produces a pulsed output and which can be generated in a variety of ways. The chapter provides a general overview of the three kinds of frequency combs studied here : bulk EO combs [14, 15], anomalous dispersion microcombs [16, 17], and coupled cavity normal dispersion microcombs [18, 19].

The fifth chapter then provides a more detailed overview of the future prospects of this research, while the sixth chapter provides a brief overview of each of the then appended Papers A-E.

1.3 General Background

Lasers [20, 21] are a well understood and established technology that provide a means towards controllable and well organized beams of light.

Originally an acronym meaning "Light Amplification through the Stimulated Emission of Radiation", today, the word has taken on a new meaning where the word laser typically refers to UV, visible, or IR single frequency outputs of temporally coherent light which, correspondingly, have very narrow spectral bandwidths. Generally speaking, a gain medium is pumped and placed inside of a low loss cavity. Then at some point, the gain medium may radiatively relax via spontaneous emission, generating new uncorrelated photons. These photons will then bounce back and forth inside the cavity, interacting with the gain medium to induce stimulated emission and thereby generate frequency and phase duplicates of the original photon(s), i.e. optical gain. Constructive and deconstructive interference in the cavity will force mode discretization, while frequency-selective elements may force single-mode operation. The result, at steady state, is a stably operating single frequency light source with low noise.

The original photons which seed the lasing process don't have to come from spontaneous emission in the gain medium. In the case of optical injection locking [6], external light from a 'master laser' may enter the cavity and provide the seed photons for coherent lasing. If there is a small enough frequency offset between the injected optical field and the unperturbed frequency of the so called 'slave laser', and if the amplitude of the injected field is strong enough to overcome spontaneous emission in the cavity, then the final output of the complete optical system will act as a frequency copy of the master laser with a fixed phase offset which depends on the frequency difference between the injected field and the slave laser's unperturbed frequency, and we say that the system is 'locked.'

On the other hand, highly coherent and low noise optical sources don't necessitate single-mode operation. Optical frequency combs [12] are a special class of laser studied at length in this work, and are defined by their many equally spaced and (importantly) mutually coherent optical tones that sit at well defined frequencies and which, in the time domain, corresponds to a pulsed laser output. They can be formed in a variety ways, including fully stabilized mode locked lasers, cascaded electro-optic modulation, and the nonlinear generation of new frequencies of light via the Kerr effect [22, 23]. Typically, they are characterized using two main parameters, the frequency spacing between optical modes (which corresponds to the repetition rate of the pulses in the time domain), and the shared frequency offset from zero for all optical modes (which corresponds to the pulse's carrier envelope offset frequency). No-

tably, however, the frequencies in question are quite mismatched. A typical frequency comb has its carrier in the visible or infrared (on the order of hundreds of THz), while its repetition rate and carrier envelope offset frequency might be on the order of MHz or GHz. This provides a direct link between the RF and optical domains which can be exploited for a huge number of applications.

1.4 General Relevance and Importance

Lasers are a relevant and important technology in our lives in ways that many of us might not imagine. Indeed, modern society would likely be impossible without the use of lasers.

From every items we handle ourselves like bar-code scanners at the self checkout, to fully integrated laser arrays on our iPhones that can create full 3D scans of the environment - lasers are all around us. I would argue, however that that the role of lasers in the fields of frequency referencing [24–28] and communications [29–31] are what drive their scientific importance today.

When transmitting data from one place to another or developing high frequency reference tones, it is often desirable to use carrier particles which are non-interacting in order to maintain the stability of the system. Conversely, when manipulating data (e.g. when doing computations), it is often highly advantageous to have particles which are strongly interacting. For these reasons, we typically use fermions (electrons) in our computers, and bosons (photons) for transmitting the generated data over long distances.

Given that a laser is, by definition, a highly coherent and well behaved photon source, it makes sense that they would find applications in a wide variety of fields where stability is desired. Not only does the generation of low noise and very predictable photon sources improve the ability of humans to communicate with one another quickly and efficiently, it also allows us to produce ultra high frequency references which can be used for applications such as optical clocks and time transfer [12], GPS [32], LIDAR [33], the detection of gravitational waves [34] and exoplanets hundreds of light years away [35], and more.

CHAPTER 2

Laser Noise

2.1 Lasers

Lasers are a mature technology which originated in the 1950's [2], and have since seen widespread adoption in the modern world. The principle of operation is as follows :

In general, when a gain medium is excited, it may either spontaneously relax (giving off heat, light, etc), or may be forced to relax in a process called stimulated emission. In this case, a resonant incident photon forces the radiative relaxation of the gain material to produce a frequency and phase copy of the original incident photon, thus generating optical gain. When placed inside of a reflective cavity, and under certain conditions, light can build up in one or many modes of the cavity to produce a coherent output that we call a laser.

2.1.1 Rate Equations

There are many kinds of lasers, but a typical semiconductor laser in single-mode operation be described mathematically as follows, using mode size and photon count normalized split equations [36–38]. Of note, these equations are often presented in photon count, but for the sake of consistency, are presented here in the mode-size normalized electric field notation [3, 39] :

$$\frac{d|E|}{dt} = \frac{1}{2}\{[G_n(N - N_0)/(1 + s|E|^2)] - \frac{1}{\tau_p}\}|E| + F_E \tag{2.1}$$

$$\frac{d\Phi}{dt} = \frac{\alpha}{2}\{[G_n(N - N_0)/(1 + s|E|^2)] - \frac{1}{\tau_p}\} - \omega_o + F_\Phi \tag{2.2}$$

$$\frac{dN}{dt} = R_p - \frac{N}{\tau_r} - [G_n(N - N_0)/(1 + s|E|^2)]|E|^2. \tag{2.3}$$

Here, the terms have the following meaning [40], with units given later in the text :

$\|E\|$	slowly varying electric field envelope
Φ	output phase
N	carrier count
G_n	gain parameter
N_0	carrier count at transparency
s	gain compression coefficient
τ_p	average photon lifetime
α	linewidth enhancement factor
ω_o	laser oscillation frequency
R_p	pump parameter
τ_r	average carrier lifetime
F_E, F_Φ	Langevin noise forces

Single mode operation can be achieved using frequency selective reflectors or absorbers in the cavity or at its mirror edges, via an external cavity, etc [1, 41]. Otherwise (as in Fabry-Perot (FP) lasers), additional terms which correspond to inter-mode energy transfer and mode partition noise may be included [1, 42], along with a set of laser rate equations for each optical mode. Noise terms are typically required for starting the process using 0 initial electric field, but may be neglected in some cases.

We first notice the term $G_n(N - N_0)/(1 + s|E|^2)$, in which a mode normalized gain parameter is multiplied by the carrier count above transparency, and then divided by a gain compression factor in order to introduce new photons into the cavity. In equations 2.1 and 2.2, this term is counteracted by the photon decay term $(-\frac{1}{\tau_p})$, where typical photon lifetimes in the cavity are many orders of magnitude longer than the total round trip lifetime of the cavity, and the cavity itself is assumed to be stable. In the electric field equation (2.1), the term which balances gain and loss is multiplied by the current electric field magnitude in the

cavity, while in the phase term, it is multiplied by the amplitude to phase conversion term (i.e. linewidth enhancement factor), α. Finally, the carrier number equation (2.3) has a pump term which adds carriers (R_p), a loss term which subtracts carriers ($-\frac{N}{\tau_r}$), and a balancing term ($-[G_n(N-N_0)/(1+s|E|^2)]|E|^2$) which links the electric field and carrier concentration equations in order to provide a restoring force.

Generalized Langevin noise forces can be included in equations 2.1 and 2.2 by adding $+F_E$ and $+F_\Phi$ stochastic noise terms. When amplified spontaneous emission (ASE) is the only noise source present, these terms can be written as follows [43] :

$$F_E = \frac{2\beta N}{|E|} + \sqrt{\beta N}\xi_E(t) \tag{2.4}$$

$$F_\Phi = \frac{\sqrt{\beta N}}{|E|}\xi_\Phi(t), \tag{2.5}$$

where β, the spontaneous emission factor, represents the proportion of ASE native to the slave laser which enters the lasing mode, and $\xi(t)$ is a stochastic noise term that varies as a function of time with mean 0 and standard deviation σ.

In simulation, these β terms can be normalized to the step size, bandwidth, and rate of radiative recombination :

$$\beta \longrightarrow \beta B B_{\text{sim}}, \tag{2.6}$$

where B is the rate of bimolecular recombination (a second order process) in the semiconductor, and B_{sim} is the simulation bandwidth.

In this case, a new term which links the carrier count and electric field via B might be needed, and is represented by a simple $+BN^2$ term added to $\frac{dN}{dt}$ to provide a restoring force on the carrier count against spontaneous emission. Similarly, a third order term which represents Auger recombination may be added. Alternatively (and as seen in the above equations and more generally in the field at large), one may linearalize the carrier loss rate term, $R(N) = AN + BN^2 + CN^3$, around the value of N at steady state operation into a single τ_r term which represents the average electron-hole recombination time, where A corresponds to the nonradiative electron hole recombination rate [44].

Similar to other noise terms, we could introduce some $F_N = \sqrt{2R(N)}\xi_N(t)$, with $\xi_N(t)$ being a stochastic noise term that varies in time with mean 0 and standard deviation σ, but this term is neglected for the remainder of the discussion [44].

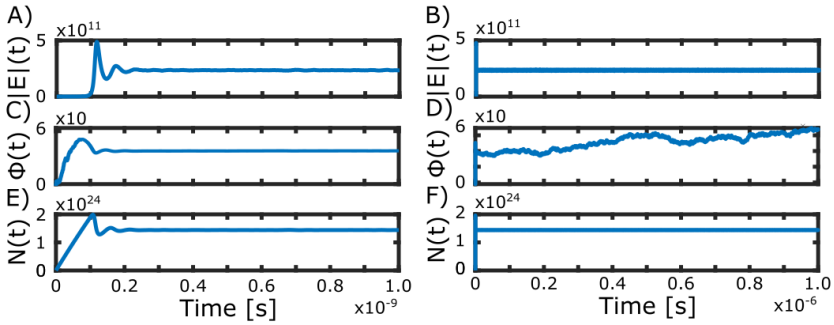

Figure 2.1: Rate equation simulations of the normalized electric field magnitude (top), phase (middle) and carrier density (bottom) for the transient turn-on dynamics (left) over a 1 ns time scale and during stable operation (right) over a period of 1 μs. Simulation parameters are provided in the main text.

Simulations of these rate equations as a function of time are given in figure 2.1, using typical parameters [44]. All values are normalized to mode size, and therefor correspond to carrier and photon densities. These are $G_n = 8 \cdot 10^{-13}$ m^3/s, $s = 1 \cdot 10^{24}$ m^{-3}, $N_0 = 1 \cdot 10^{24}$ m^{-3}, $\alpha = 3$, $A = 1.0 \cdot 10^{-9}$ s^{-1}, $B = 1.0 \cdot 10^{-16}$ m^{-3}s^{-1}, $\tau_p = 3.0 \cdot 10^{-12}$ s^{-1}, $R_p = 1.0 \cdot 10^{34}$ m^{-3}s^{-1}, and $\beta = 1.0 \cdot 10^{-3}$. Third order recombination is ignored ($C = 0$), a time step of 1 picosecond is used, and simulations advance for 1 microsecond. Initial conditions are all set to 0, driving current is turned on at $t = 0$, and ASE terms are used to seed the lasing process. In this case, the output power is given by $P = K v_g \mathrm{A_{eff}} h f |E|^2$ where K is the output coupling term, v_g is the group velocity, and $\mathrm{A_{eff}}$ is the effective modal area. Given that random Langevin forces are included, 4$^{\text{th}}$ order Runge-Kutta simulations are used [45].

Relaxation oscillations are readily apparent after activation of the laser, and the effects thereof are seen in the electric field magnitude, phase, and carrier count. Furthermore, the carrier count and electric field are shown be to be quite stable over long time scales, while the output phase is not. This is due to the lack of restoring force on Φ, and results in the linewidth broadening of the laser output caused by phase accumulation. Both intensity and phase/frequency noise will now be discussed at length.

2.2 Intensity Noise

The laser's output power is determined by the strength of the electric field square magnitude, multiplied by some output coupling term that picks off a small portion of the optical field oscillating in the cavity. All else being equal, the final output power is determined primarily by the normalized driving current applied to the gain medium (R_p from equation 2.3), assuming operation well away from the gain compression region.

2.2.1 RIN

Whether it comes from the driving current, from the random nature of gain and loss, or from fluctuations native to the laser itself, there will always be some degree of variation in output power. When this noise is normalized to the average output power, it is called relative intensity noise (RIN) [46], and corresponds to power fluctuations on the A(t) component of the the optical wave equation for a single-frequency laser, i.e.

$$A(t) = \{A_0 + \Delta A(t)\} e^{i\omega_c t + \Delta\phi(t)}. \tag{2.7}$$

When the RIN of a laser source is measured as a function of frequency, the resulting power spectral density (PSD) measurement is given in units dB/Hz and communicates information about whether intensity fluctuations are rapid (such that they might be averaged away by a slow photodetector), slow (such that they might not matter for short detection periods), or present in large amounts only at a few select frequencies.

Mathematically, the frequency dependent RIN PSD is given by

$$S_{\mathrm{RIN}}(f) = \frac{2}{P_{\mathrm{avg}}} \int_{-\infty}^{+\infty} \langle \delta P(t) \delta P(t+\tau) \rangle e^{i2\pi f\tau} d\tau, \tag{2.8}$$

where P_{avg} is the average optical power and δP represents the time dependent power fluctuations which we are trying to quantify.

In general, RIN spectra can be quite complex. It is for this reason is is often advantageous to compress intensity noise into a single root mean square (rms) value :

$$\left.\frac{\delta P}{P_{\mathrm{avg}}}\right|_{\mathrm{rms}} = \int_0^{\Delta f} S_{\mathrm{RIN}}(f) df, \tag{2.9}$$

where Δf is the receiver bandwidth.

Importantly, RIN can come from a variety of sources, both internal and external. For instance, in fiber or semiconductor lasers, RIN might be transferred from the pump onto the final output beam, but might also come from ASE inside the gain medium, technical noise stemming from thermal fluctuations in the control system or optical path length, fluctuations in diode resistance, etc [47, 48].

To some extent, RIN in a single frequency laser can be reduced in a relatively straightforward manner. For instance, feedback loops on the control systems which govern the device temperature, driving current, etc. can be used to mitigate and reduce technical noise. Alternatively, an intensity modulator such as an Mach-Zehnder modulator (MZM) [49] or acousto-optic modulator (AOM) [50] can be used in either feedback or feedforward schemes to directly compensate for changes in intensity. Both of these devices are discussed later in the text.

A typical RIN spectrum might look like the PSD in figure 2.2, which is calculated from the the simulations in figure 2.1, and is normally presented in a log-log plot. This RIN spectra demonstrates white noise, the relaxation oscillation peak which arises due to the gain medium not responding instantly to the electric field, and so-called pink noise. Each of these will now be discussed.

2.2.2 White Noise / Shot Noise

White noise corresponds to any noise source for which the intensity of noise is independent of frequency. It may arise in laser systems due to many factors, ranging from thermorefractive fluctuations and the random nature of absorption and gain, to spontaneous emission and various quantum effects, but one important type of quantum noise is called shot noise [1, 29, 51]. This is a type of laser amplitude noise which arises during the process of photodetection due to the quantized nature of photons. It can be understood by considering the optical field as a series of small, individual packets of energy which must therefore occur at the detector at random discrete time instances, instead of as a continuous flow. In this case, the single sided PSD of relative intensity noise is given by

$$S(f) = 2hf\frac{1}{P_{\text{avg}}}, \tag{2.10}$$

where hf is equal to the photon energy, and P_{avg} is the average optical power. Here, it can be seen that by increasing the power, we reduce the

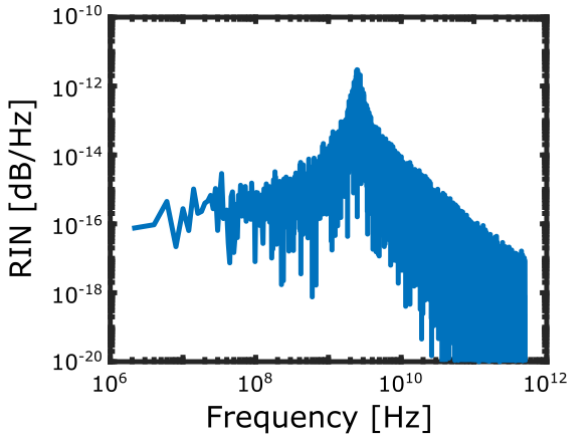

Figure 2.2: A typical, although idealized, RIN PSD which is calculated from the simulations above and is used to demonstrate white noise, pink noise, and the relaxation oscillation peak that shows up as function of the rise and fall time of photons and carriers, respectively. Here, shot noise is not considered.

shot noise. Moreover, like all random processes following a Poissonian distribution, the corresponding single side band noise PSD will be white (flat) as a function of frequency [52]. The corresponding rms value of noise current induced by shot noise on a photodetector is given by $\sigma_s^2 = 2e\langle I_e\rangle\Delta f$, where e is the electron charge, $I_e = I_p R$ is the induced electric current equal to the photocurrent multiplied by the detector responsivity, and Δf is the bandwidth of the receiver [29].

2.2.3 Relaxation Oscillations

Relaxation oscillations occur in most types of lasers where the upper state lifetime is much longer than the cavity damping time (keeping in mind that resonators with high quality factors have low damping times). This corresponds to a system which might experience a fluctuation, and then return to the steady state solution in an oscillatory manner, with some kind of repeating overshoot combined with some amount of damping applied to the oscillation. Physically, this can be understood as the gain medium not acting quickly enough on the light traveling within it, thereby producing damped overshoots as it tries to reach steady state after the applied change [1, 3, 4].

Ignoring gain compression and using a linear stability analysis, the

frequency of this oscillation, ω_{RO} is given by

$$\omega_{RO} = \sqrt{\frac{\mu - 1}{\tau_r \tau_p}} \tag{2.11}$$

where μ is the threshold normalized pump parameter for coherent lasing of the semiconductor device ($\mu = R_p/R_{p,\text{threshold}}$).

2.2.4 Pink Noise

Pink noise is a broad term that corresponds to a large variety of noise sources which decrease in strength as you move towards the blue (high frequency) end of the spectrum, and increase in strength as you move towards the red (low frequency) end of the spectrum . These sources can be said to follow a $\frac{1}{f^m}$ spectrum, with $m > 1$ [1,3,4]. In general, these are the noise sources which dominate over long time scales, and are therefore particularly important for applications requiring long term stability such as optical references for spectroscopy, communications, clocks, etc.

In general, $\frac{1}{f}$ noise will be present in all electronic circuits due to flicker noise, a kind of DC current related fluctuation which is variously attributed to resistance fluctuations, surface traps, and more [53].

Another important source of pink noise in natural systems is Brownian noise, named for Robert Brown (as opposed to the color). This kind of noise scales like $\frac{1}{f^2}$ and corresponds to random walk generated by adding white noise to each point before calculating the next - as opposed to white noise which is added in bulk after calculations, and is useful for modeling the random walk of a laser's operating frequency or the Brownian motion of carriers inside the gain medium [54].

2.3 Phase and Frequency Noise

Phase and frequency noise are intimately connected, given that the instantaneous frequency is defined as the time derivative of phase

$$\nu(t) = \frac{1}{2\pi}\frac{d\phi}{dt}, \tag{2.12}$$

we can write a relationship between the power spectral densities of of the two as

$$S_\Phi(f) = \frac{1}{f^2} S_f(f), \tag{2.13}$$

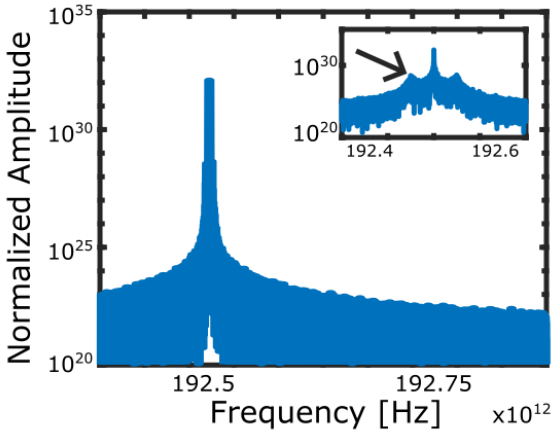

Figure 2.3: The calculated optical spectrum corresponding to the above simulations, showing the normalized amplitude as a function of optical frequency. Here, the inset is a zoomed-in version of the main figure, used to illustrate how relaxation oscillation peaks (indicated by an arrow on one side of the main peak) transfer from the intensity domain to the output optical spectrum.

where S_Φ and S_f are the frequency dependent single sided power spectral densities of phase and frequency noise, respectively. Importantly, this highlights the fact that white phase noise corresponds to frequency dependent frequency noise [55].

2.3.1 Linewidth

The optical spectrum can be derived from the Fourier transform of the electric field autocorrelation function, according to the Wiener-Khinchin theorem (seen in figure 2.3). Here, phase and frequency noise manifest as the broadening of the laser's spectral linewidth [56, 57], and in some instances, it may be advantageous to quantify this broadening in the form of a single parameter, which may or may not include various contributions according to the definition of linewidth used. Of note, the normalized amplitude provided for optical spectra in this text are given relative to photon energy and step size of the simulation, as well as the time length of the simulation via the autocorrelation function.

Originally, laser linewidth was defined by the Schawlow-Townes approximation [41], also called the fundamental linewidth, and refers to the

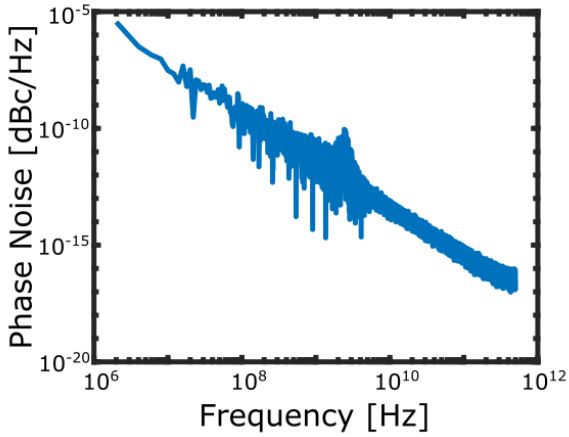

Figure 2.4: Normalized phase noise, $S_\phi(f)$ as a function of offset frequency from the carrier, calculated using the simulation parameters given above.

case of minimum possible noise (quantum noise) [58, 59], as given by

$$\Delta\nu_L = \frac{R_{\text{decay}} - R_{\text{st}}}{R_{\text{decay}}}\Delta\nu_c, \tag{2.14}$$

where R_{decay} represents the rate of photon decay in the cavity, R_{st} gives the rate of stimulated emission, and $\Delta\nu_c = (2\pi\tau_p)^{-1}$ represents the full-width half-max (FWHM) Lorentzian linewidth of the passive resonator mode in which gain occurs.

This approximation assumes a purely Lorentzian spectral shape, which corresponds to white noise on the frequency noise PSD. This is never the case in reality, where $\frac{1}{f^m}$ noise and intensity to phase noise transfer will inevitably play a role. Thus, (ignoring all other components), any real laser's spectral line will look like some combination of a Gaussian and Lorentzian function (i.e. a Voigt profile). A typical phase noise spectrum, calculated from the simulations above, is seen in figure 2.4.

To address this non-Lorentzian deviation from the ideal spectral profile, there exist a variety of definitions for linewidth which include higher order or noisy components which may contribute to laser linewidth [60]. One such approach [61] is the integrated linewidth definition given below, where the linewidth is defined as the phase noise integral from infinity, down to whichever frequency, ν_{int}, corresponds to an area under the

curve of $\frac{1}{\pi}$, such that

$$\int_{\nu_{int}}^{\infty} S_\phi(f)df = \frac{1}{\pi}. \tag{2.15}$$

Other approaches to define linewidth make use of various fit methods. One example is the beta line approach, for instance [62], which makes a strong assumption of the frequency noise PSD profile being either fully Gaussian or fully Lorenzian over some portion of the PSD, and therefore fail to address deviations from the assumed Voigt profile (such that the method fails under heavy technical noise). The integrated linewidth definition is more robust however, and is therefore preferable in many contexts, although it should be noted that it does tend to provide larger values of linewidth and is therefore often not provided in papers or technical specifications.

On the other hand, when trying to investigate certain unavoidable and underlying properties of a laser, for instance, it is still often very useful to isolate the analysis from any technical or $1/f^m$ components, and focus interest solely on the lowest / white-noise limit of the system (i.e. the Lorentzian / Schawlow-Townes approximation), since this provides important information about properties such as fundamental quantum noise [63]. This kind of analysis is also very useful in communications and other short time window measurements, where slow drift can often be accounted for using digital signal processing (DSP) [64].

In figure 2.5, three different methods of measuring linewidth are presented graphically to provide an intuitive explanation of the process. The integrated linewidth approach gives a value of approximately 1.5 kHz, while two fits to the same data are provided following the method outlined in [65] (which fits the data to white frequency noise in order to estimate the fundamental linewidth), the first of which includes excess noise and gives a value of approximately 710 Hz, and the second of which attempts to remove excess noise and provides a fundamental linewidth of approximately 120 Hz - more than 10 times less than the integrated linewidth and 5 times less than the fundamental linewidth as calculated including technical noise. It should be clear then, that any discussion of linewidth requires careful reading and a clear understanding of how the value was recovered, and what assumptions, if any, were made.

To some extent, phase noise, like RIN, may be controlled and reduced in a rather straightforward manner, such as by using feedback loops onto the laser frequency control of the laser, or by implementing feedback and feedforward schemes which rely on an external modulator [66–69].

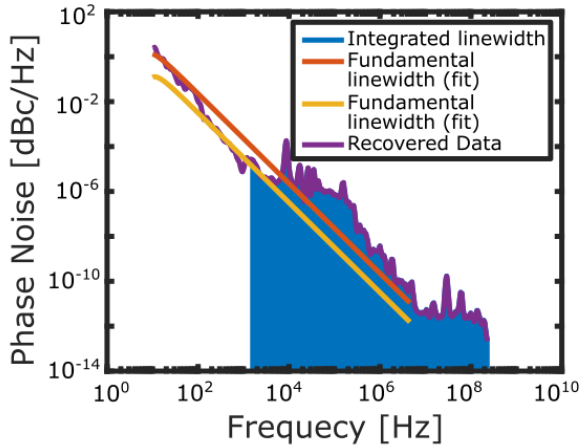

Figure 2.5: A visual representation of various methods for approximating laser linewidth from phase noise data. The integrated method (blue) corresponds to a linewidth of approximately 1.5 kHz. The first fit type (orange) includes excess noise and gives a value of approximately 710 Hz, while the second fit method attempts to ignore added noise and gives a recovered linewidth of 120 Hz.

2.4 Mutual Coherence

Although noise measurements of a single optical tone are important, it is often just as important to measure the degree to which two tones are correlated.

The mutual coherence of two optical tones in the time domain, $x(t)$ and $y(t)$, is defined by [70]

$$\gamma^2_{1,2}(f) = \frac{|S_{1,2}(f)|^2}{S_{1,1}(f)S_{2,2}(f)}, \tag{2.16}$$

where $S_{1,2}$ is the cross spectral density of the signal, $S_{1,1}$ and $S_{2,2}$ are the power spectral density of the two signals, $x(t)$ and $y(t)$, in question, and where the cross spectral density and power spectral density are defined as the Fourier transform (FT)s of the cross-correlation and auto-correlations of the time domain signal, respectively.

Importantly, mutual coherence is a quantity which does not include the noise properties of each individual tone, and instead tries to quantify the amount of noise which is not common between the two measurements. For instance, if both tones suffer from technical noise due to a 1

MHz ground loop, this will not degrade the degree of mutual coherence between the two.

To measure mutual coherence, two signals of equal power can be measured separately, and then analysed in post processing in the time domain. Alternatively, the two signals may be directly beaten together and the an analysis of the beat note's noise may be considered along with the noise power spectral density of each individual beam.

Under certain conditions, mutual coherence between tones can be forced by locking two tones together. This can be done using various techniques, but two common methods - proportional, integratal, and derivative (PID) control loops and OIL - are discussed at length later in the text.

2.5 Measurement Techniques

2.5.1 Intensity Noise Measurements

Intensity noise measurements are typically quite straightforward [46], and can be done by directly sending light onto a photodiode. However, one must be careful to calculate the shot noise limit, given that shot noise is directly related to the amount of light received. Furthermore, the receiver as a whole may introduce additional noise in the form of thermal noise, flicker noise, radio frequency (RF) cavities which induce back reflections, noise from the electronic driving current being written onto the output, or due to electronic noise from built-in RF amplifiers, among other sources. It is for this reason that one must be careful to select low noise devices with adequate bandwidth and ensure measurements are performed above the frequency dependant noise floor [71].

2.5.2 Phase and Frequency Noise Measurements

There are several approaches for the measurement of phase and frequency noise. The first class of measurement techniques rely on beating a noisy source against what is known to be an exceptionally low noise source such that any additional noise can be attributed to the noisy signal being measured. Similarly, there are a variety of techniques which rely on using three sources in order to reduce the required assumptions and aide in the measurement of low noise lasers [72]. These measurement schemes are referred to as heterodyne measurements, given that multiple distinct signals are beat against one another, and can be quite simple to

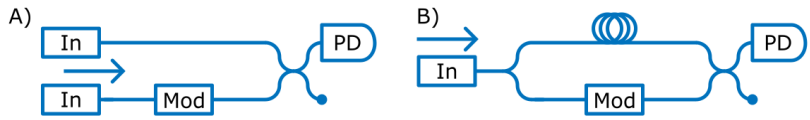

Figure 2.6: A) Heterodyne and B) Homodyne (self-heterodyne) measurement optical schematics. In both cases, the bottom arm is modulated to push the beat note further from baseband (DC) to avoid low frequency components and reduce signal to noise ratio (SNR) at the output.

implement, but are not always appropriate when dealing with very low noise sources.

The second class of measurements, called homodyne (or self-heterodyne) measurements begin by splitting the signal in two and passing one portion through a delay line sufficiently long such that it is either fully or partially decoherent with its undelayed copy [73, 74]. The two signals are then mixed together, and a beat note is measured. From this, one can measure the phase noise PSD directly, or measure the electronic spectra on an electric spectrum analyser (ESA) and extrapolate a linewidth measurement. Importantly, in such measurements the beat signal will often be near to baseband, and as such, should be frequency shifted using an AOM to avoid electronic measurement errors.

Self-heteroydyne approaches are generally valid, but extra care must be taken to select an appropriate delay length and to isolate each arm from external noise sources. For lasers with very low phase / frequency noise (P/FN), impractical lengths of delay line might be needed for full decoherence of the two arms, which may introduce additional technical noise or loss such that accurate measurement is rendered impossible. Instead, partially decoherent measurements are often required.

A simulated example of the electric spectrum for partially decoherent beams beating against one another is presented in figure 2.7. Here the linewidth of the laser is 212 Hz (a coherence time of 1.5×10^3 seconds), the delay line's length is set to 25 km, and any excess noise not related to the laser linewidth has been removed. The carrier frequency is set to 192 THz, the fiber index of refraction is set to 1.4682, and the AOM driving frequency is set to 25 MHz. A schematic outline of the optical setup for such a measurement can be found in [Paper A]. In such a situation, the linewidth is given by a complex fit function, or can be estimated by measuring the relative strength between peaks and troughs of the

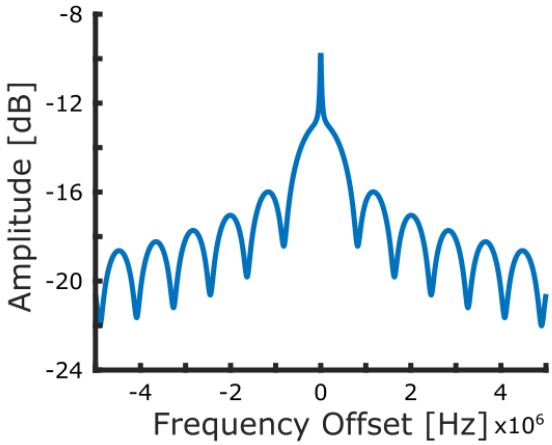

Figure 2.7: The electric spectrum of subcoherent beating, which might be recovered from the ESA in a delayed self heterodyne experiment. Here, the spacing between subsequent lobes is set by the interferometer, while the depth of these lobes is related to the degree of coherence. From this, one can estimate the laser linewidth.

spectrum's side lobes, as described below.

The spectrum of subcoherent beating in a delayed self-heteroydyne experiment is given as follows [75, 76] :

$$S(\omega,\tau) = \frac{A\tau_c}{1+\Delta\omega^2\tau_c^2}[1 - [|\tau|e^{-|\tau|/\tau_c}\cos(\Delta\omega) + \frac{\sin(\Delta\omega)}{\Delta\omega}]] + \pi A e^{-|\tau|/\tau_c}\delta(\Delta\omega), \tag{2.17}$$

where $A = \frac{1}{2}P_o^2$, $\Delta\omega = \omega - \Omega$, Ω is the AOM driving angular frequency, τ is the delay time between arms, τ_c is the coherence time of the laser, and P_o is the optical power.

Given how difficult such a curve might be to fit, it is often easier to simply measure the phase/frequency noise PSD and directly integrate, although doing so is only truly valid from the inverse time delay, $\frac{1}{\tau}$, up to the bandwidth of the detector used. In the case where this integration does not reach the $\frac{1}{\pi}$ threshold from equation 2.15, the curve is fit using white and pink noise as extrapolated from the given data set, or simply said to be under some threshhold linewidth.

Alternatively, one can make a few assumptions regarding the fre-

quency dependence of noise properties outside of the measurement bandwidth, as per [76,77], and find that the amplitude difference between the first peak and trough for the subcoherent spectra in the figure above, ΔS, is approximated by

$$\Delta S \approx 10\log_{10}\frac{16c}{9\pi nL\Delta\nu}, \tag{2.18}$$

from which the linewidth can be derived, where n is the index of refraction and L is the length of the delay line. In this case, $\frac{c}{nL}$ represents the inverse time delay.

Finally, for very low noise signals, phase and frequency fluctuations can be transferred into intensity fluctuations via interference in a Michaelson interferometer, as seen in [Paper D]. By measuring the amplitude of the sinusoidal output on a photodiode, and knowing the fixed frequency of oscillation, the measured optical power fluctuations can be converted into the frequency fluctuations of the optical signal. This assumes that the recovered trace remains within a narrow range around the quadrature point such that we may make a linear approximation of the sine wave, and that the FSR of the interferometer is both well known and stable (therefore requiring vacuum systems, temperature stabilization, optical time domain reflectometry (OTDR) measurements, etc).

2.6 Control Mechanisms

It has been previously mentioned that all three, intensity noise, phase and frequency noise, and mutual coherence may be improved up using various control mechanisms, and it is therefore worth discussing some of the ways in which light from a coherent source can be modulated in order to improve its noise properties or to encode information onto the beam.

2.6.1 Direct Current and Temperature Modulation

The simplest form of semiconductor laser control is direct current modulation and is performed by varying the R_p pump parameter from equation 2.3. In fact, this kind of modulation is so common that most commercial systems come with a built-in external modulation port which can be used to variously mix signals with the standard driving current to produce sine waves, square waves, etc.

Of course, there are several downsides to direct modulation. Firstly, by increasing the amount of driving current, additional carriers in form of electron hole pairs are added to the cavity, thereby changing the index of refraction in turn. Moreover, additional light is introduced to the cavity which corresponds to higher absolute losses and therefore an increase in temperature and thus both an increase in thermal noise and a change in refractive index. All together, this means that a change in driving current is necessarily accompanied by a change in effective cavity length, optical phase, and oscillating frequency [78].

Similarly, most modern laser systems offer direct control of the temperature via an external port or some internal control electronics. This makes sense, given that we already know temperature fluctuations will cause random drift in the lasing frequency and therefore should normally be mitigated. Unfortunately, thermal changes are quite slow (on the order of kHz-MHz) and are therefore not particularly useful for high speed modulation, although can still be used in control systems to account for very low frequency pink noise and the Brownian motion of random laser walk [79].

2.6.2 External Phase Modulation

The phase and amplitude of a laser source can be modulated externally as well. There exists various crystalline materials which exhibit a symmetry break in their lattice and which can be used for such purposes. When an electric field is applied to the material, this creates an atomic scale deformation in the crystal which changes the index of refraction as a function of the strength and direction of the applied field. Importantly, because these crystals are non centro-symmetric, the direction and polarization of light propagation are quite important [51, 80].

When passing through such a material, the phase of light may therefore be modulated to produce sidebands, encode information onto the light, etc. We can write a simple expression to define the action of such a modulator as follows :

$$E_{\text{out}} = E_{\text{in}} e^{i\pi \frac{V(t)}{V_\pi}}, \tag{2.19}$$

where $V(t)$ is the applied voltage and V_π corresponds to the amount of voltage required to produce a single π phase shift.

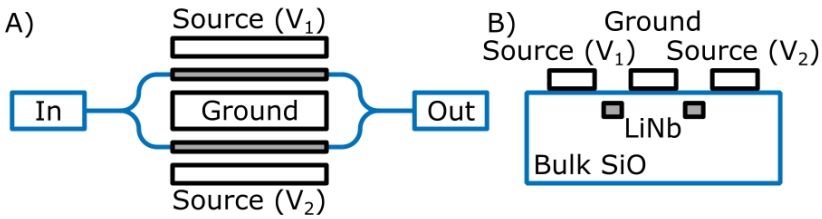

Figure 2.8: A top (A) and side (B) view of an idealized, chip based MZM. Here, an optical input is split into two arms - each of which produces phase modulation via the electro-optic effect. This is done by generating an electric field between the ground and source which thereby modulates the Lithium Niobate (LiNb). Not pictured here is the mechanism required for fixing $V_1(t) = -V_2(t)$ for pure amplitude modulation.

2.6.3 External Amplitude Modulation

Furthermore, phase modulation may be used to generate amplitude modulation. This is typically done using a single source of light which is divided into two equal beams, each of which passes thru its own phase modulator, as seen in figure 2.20. Afterwards, the two modulated signals are recombined and the result is expressed as follows (assuming equal V_π and equal path length) :

$$\begin{aligned} E_{\text{out}} &= \frac{1}{2}E_{\text{in}}\left(e^{i\pi\frac{V_1(t)}{V_\pi}} + e^{i\pi\frac{V_2(t)}{V_\pi}}\right) \\ &= \frac{1}{2}E_{\text{in}}[\left(\cos(\pi\frac{V_1(t)}{V_\pi}) + \cos(\pi\frac{V_2(t)}{V_\pi})\right) \\ &+ i\left(\sin(\pi\frac{V_1(t)}{V_\pi}) + \sin(\pi\frac{V_2(t)}{V_\pi})\right)]. \end{aligned} \tag{2.20}$$

In the special case where $V_1(t) = V_2(t)$, the system collapses to a simple phase modulator, which makes sense given the symmetry of the system.

On the other hand, in the case where $V_1(t) = -V_2(t)$, the sine functions cancel (due to the nature of odd functions), and we're left with pure amplitude modulation.

Alternatively, instead of using electro-optic principles to create intensity modulation, one may use an AOM. As seen in figure 2.9, the device works by running a longitudinal acoustic wave (comprised of compressions and rarefactions) through a crystal using some kind of piezoelectric

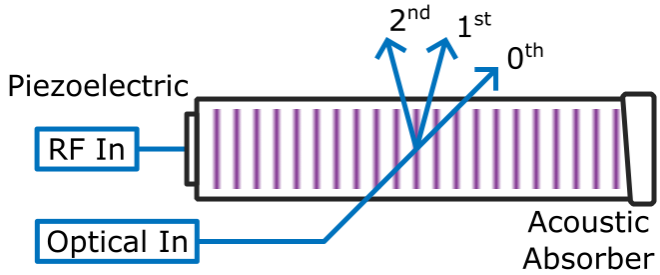

Figure 2.9: A simplified model of an AOM, including an RF driving field which modulates a piezoelectric material which, in turn, is acoustically coupled to some crystalline material. Compressions and rarefactions travel from the piezoelectric through the AOM and to the opposite end, where acoustic waves are then scattered, absorbed, etc. Simultaneously, an optical beam is sent through the device at an offset angle, and is Doppler shifted by the traveling acoustic wave to produce diffraction at fixed angles determined by the frequency of modulation.

transducer attached at one end. This modulates the index of refraction of the material, producing diffraction at fixed angular offsets from the output of the crystal. Adjacent angles are separated by $\Theta_B = \frac{\lambda}{\Lambda}$, where λ and Λ are the optical and acoustic wavelengths, respectively. The 0^{th} order (or transmitted portion) contains the un-shifted frequency, while the m^{th} order operates at $f = f_0 + m\Delta f$, where Δf is the Doppler frequency shift induced by the traveling acoustic wave [51].

2.6.4 Control Loops

In order to actually use internal or external modulation to stabilize the intensity or phase noise of a laser, control loops are typically required. These loops come in a variety of forms, including feedback and feedforward schemes. One particularly common method is the PID loop [81] (seen in figure 2.10), which consists of a (P)roportional, (I)ntegral, and (D)erivative component of the control signal, written as

$$u(t) = K_P e(t) + K_I \int_0^t e(\tau)d\tau + K_D \frac{de(t)}{dt}, \tag{2.21}$$

where K_P, K_I, and K_D are the gain parameters, and $e(t) = \tau(t) - y(t)$ is the error function, defined as being equal to the set point, $\tau(t)$, minus

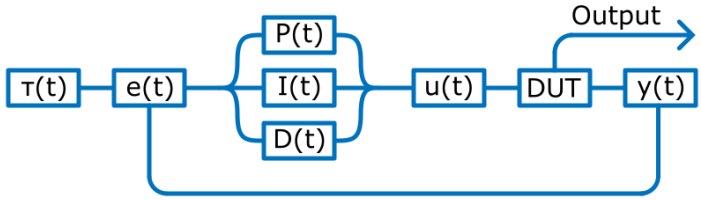

Figure 2.10: Schematics of a typical PID loop which measures a process variable of some DUT, y(t), and compares this to a given set point, τ(t), to generate an error function, e(t). Proportional, integral, and differential gain functions are then applied to the error in order to generate a control function, u(t), which is fed into the DUT, thus changing the process variable which is then again compared to the set point, and so on. Such a loop, when K_P, K_I, and K_D from equation 2.21 are chosen properly, is able to stabilize the system against fluctuations.

the process variable used for comparison, $y(t)$, and where the control function, $u(t)$ acts on the device under test (DUT).

In such a scheme, the proportional component corresponds to the instantaneous, time-delayed, difference in value from the measured and set points, while the integral value term considers past behavior and the derivative term tries to predict future system behavior [81].

When properly tuned [82], the control signal acts on the process variable in such a way that the error signal is ideally reduced to zero. The speed at which this occurs is determined primarily by the loop length and the amplitude of $u(t)$, which is set by the gain parameters K_P, K_I, and K_D. When these parameters are not properly tuned, the system will either fail to stabilize, or will do so in an erratic or unwanted way. For instance, if gain is much too high, the system might overshoot, generating oscillatory behavior in the process variable as the system repeatedly tries to reach the set point. If gain is too low, the system might fail to respond properly to an error at all and never lock.

In general though, as seen in figure 2.11, there will always be some tradeoff between the speed at which the loop can adjust to a given fluctuation (determined by the gain parameters and effective loop length), and the stability of the system. A system that responds quickly tends to overshoot and generate oscillations, while a system that responds too slowly tends to undershoot and fails to account for rapid fluctuations or adequately reduce the noise. This simple fact means that a PID loop with

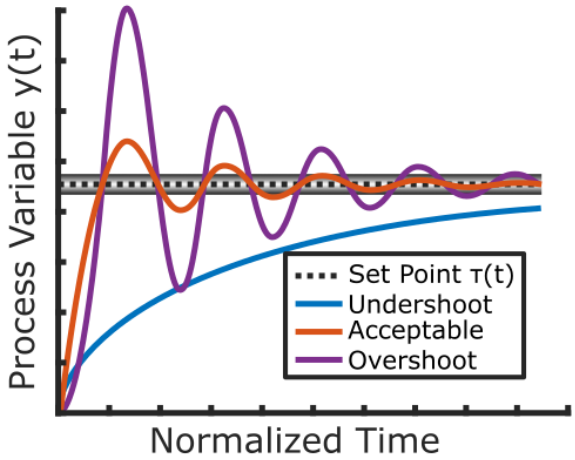

Figure 2.11: Time trace of the measured process variable, y(t), while the PID loop is active. Seen here are the three typical behaviors of PID locking near the optimal set point, including undershoot (gain too low), acceptable performance (balanced gain), and overshoot (gain too high).

fixed gain parameters will nearly always fail to provide optimal control over the long term, and dynamic parameter selection is preferred.

Finding the right combination of gain parameters can be difficult [83], but there exists a general method to do so. First, all gain parameters, K_P, K_I, and K_D, are set to zero. Then, the proportional gain is increased to the point that strong oscillations are present, and is then reduced by half. The integral gain is then increased by some small amount, and the first step is repeated to find a new proportional gain. This adjustment of the P and I parameters is complete when the system stops improving, at which point, the derivative term is included, and the whole process repeats itself. After several iterations of this process, stable locking should be achieved. Often, all three terms are not needed, and simple proportional gain or proportional and integral gain alone are enough to stabilize the system.

CHAPTER 3

Optical Injection Locking

3.1 Injection Locking

There is a ubiquitous need in the scientific community for improved ways to amplify light in a way that produces high gain with low added noise.

Traditional methods of optical amplification like semiconductor optical amplifier (SOA)s [84] and erbium-doped fiber amplifier (EDFA)s [85] work by injecting energy into a gain medium and then inducing stimulated emission via an incident field to produce amplification of the injected light. Although classical optical amplifiers can produce high gain given a sufficiently long active medium, they suffer from noise buildup in the system as ASE accumulates over the length of the gain medium alongside the light you actually wish to amplify.

A simple approach to mitigate the impact of ASE build up in long amplifiers might be to place a narrow-band bandpass filter (BPF) after the amplifier in order to attenuate unwanted optical power, but this comes with significant and obvious downsides [29]. A more advanced approach might be to place the gain medium inside of a high Q-factor optical cavity while continuing to pump the device with the light you wish to amplify, such that the optical cavity itself filters away the majority of unwanted ASE noise power at each round trip in order to preemptively avoid the buildup of noise as opposed to trying to filter it away after the fact. This is the approach used in OIL [6].

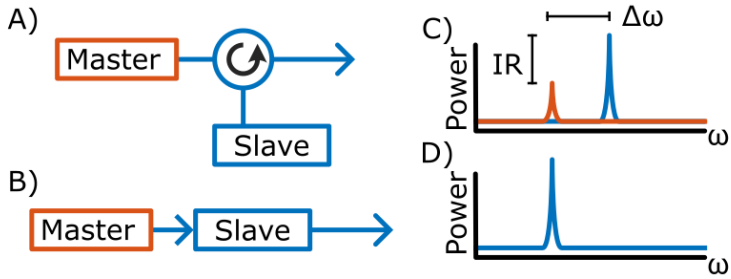

Figure 3.1: A) Reflection type and B) transmission type optical injection locking, along with an idealized picture of the slave laser output (blue) and master laser input (orange) when C) unlocked and D) locked. In C), $\Delta\omega$ and IR (defined in the text) are marked to help the reader visualize key parameters which determine whether or not the system will lock.

Conveniently, if there is a small enough frequency offset between the injected optical field (the master laser) and the natural frequency of the unperturbed gain cavity (the slave laser), and if the amplitude of the injected field is strong enough to overcome the natural oscillations in the cavity which generate the slave laser's undisturbed output, then the final output of the complete optical system will act as a frequency copy of the master laser with a fixed phase offset which depends on the frequency difference between the injected field and the slave laser's output optical field.

This process is called injection locking, and can be thought of more generally as a phenomenon that may occur in any physical system of two (or more) harmonic oscillators which are somehow uni- or multi-directionally coupled and whose oscillations can become frequency matched to one another due to this energy transfer [6].

3.1.1 Background

Injection locking was originally discovered in the mid 17^{th} century by a horologist who noticed that two of his recently invented pendulum clocks sitting on the same table are able to sometimes spontaneously self-synchronize. In this case, the two pendulums correspond to a generalized harmonic oscillator, and mechanical vibrations traveling through the wood provide a link for energy transfer between them. In the case of frequency interference without complete frequency locking, the effect is calling injection pulling [86]. The effect is seen not just in clocks and

lasers, but is used extensively in voltage controlled oscillators to synchronize various electronic components [87]. Of note, this is a frequency selective and narrow-band process, and therefore not applicable in all situations.

3.1.2 Applications

Optical injection locking (OIL) in particular, has a variety of uses, notably i) its ability to force noisy slave lasers to act as high quality frequency copies of a low noise master laser for optical reference distribution, ii) it's ability to reduce chirp in intensity modulation schemes [88], iii) it's ability to extend the modulation bandwidth of the slave laser [89, 90], and iv) it's ability to simultaneously amplify and filter light for applications such as tone selection, pump recovery and narrowband optical amplification [Papers A-B, & E].

Although OIL's ability to force noisy slave lasers to act as copies of a low now noise master laser is quite apparent, it's other applications require a more subtle explanation. For instance, OIL's ability to reduce chirp in direct modulation schemes relies on the fact that the OIL rate equations (seen below) offer a restoring force for the electric field, but not the phase difference. This means that the intensity at the output will be primarily determined by carrier concentrations in the slave laser and not by the strength of the injected field, and therefore, so long as there is enough power to lock the device, the intensity can be modulated freely without significantly changing the frequency at the output [91]. This is in direct contrast with traditional direct modulation where a change in the pump parameter, R_p, will simultaneously induce a strong change in effective refractive index and therefore oscillating frequency. Here, so long as the slave laser always remains within the locking bandwidth of the master, very little frequency modulation will accompany the intensity modulation.

Similarly, OIL's ability to extend the modulation bandwidth of a semiconductor laser requires a slightly more subtle explanation. Here, the injected field reduces the carrier count by some amount, ΔN, which in turn red shifts the cavity's oscillating frequency. This shifts the resonant beat note between the cavity and emitting frequencies to higher frequencies, effectively extending the modulation bandwidth of the device [92].

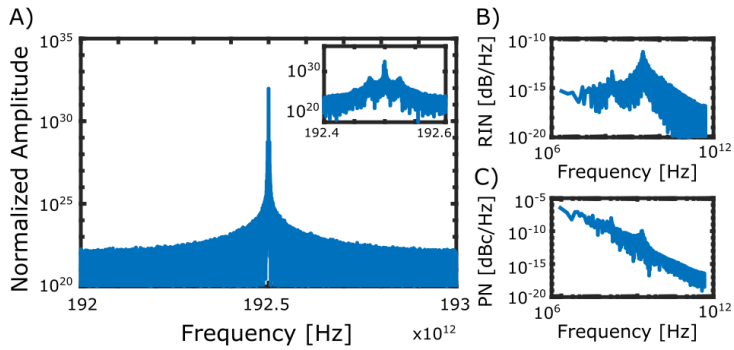

Figure 3.2: The recovered optical spectra (A), RIN (B) and phase noise (C) for failed optical injection locking using the same parameters for the slave laser as given in Chapter 2, and with $\Delta\omega$ equal to twice the locking bandwidth.

3.2 Rate Equations

Mathematically, we can express the process of OIL in a typical semiconductor laser as follows [43, 44] :

$$\frac{d|E|}{dt} = \frac{1}{2}\{[G_n(N-N_0)/(1+s|E|^2)] - \frac{1}{\tau_p}\}|E| + \kappa|E|_{inj}\cos(\Psi) + F_E \quad (3.1)$$

$$\frac{d\Psi}{dt} = \frac{\alpha}{2}\{[G_n(N-N_0)/(1+s|E|^2)] - \frac{1}{\tau_p}\} - \Delta\omega - \kappa\frac{|E|_{inj}}{E}\sin(\Psi) + F_\phi \quad (3.2)$$

$$\frac{dN}{dt} = R_p - R(N) - [G_n(N-N_0)/(1+s|E|^2)]|E|^2, \quad (3.3)$$

using the same notation seen in Chapter 2, but here with κ being the injection rate, E_{inj} being the magnitude of the injected field, Ψ being the phase offset between the master and slave lasers, $\Delta\omega$ being the frequency difference between master and unperturbed slave laser, and with the carrier decay term $R(N) = AN + BN^2$ (ignoring 3$^{\text{rd}}$ order recombination).

Simulations are shown of the optical spectra, RIN, and phase noise in the case of an unlocked (figure 3.2) and locked (figure 3.3) slave laser. The phase noise at the output of the slave laser is significantly improved

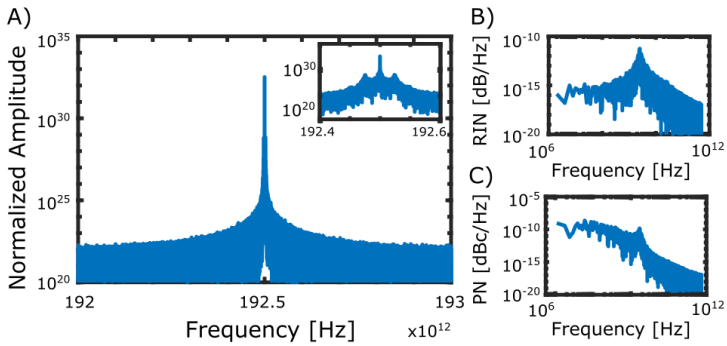

Figure 3.3: The recovered optical spectra (A), RIN (B) and phase noise (C) for optical injection locking using the same parameters for the slave laser as given in Chapter 2, and with $\Delta\omega$ equal to one quarter of the locking bandwidth.

in the case of locking to a low noise injected signal, resulting in a significant reduction in optical linewidth at the output. Moreover, a secondary peak can be seen in the RIN and phase noise spectra which corresponds to the beat note between the slave laser output field and injected field.

Of note, the mathematical model presented here is identical to the case of an external cavity laser [93], where E_{inj} is said to be a delayed copy of the output signal such that one may replace E_{inj} with $e^{i\phi}E(t-\tau)$, where τ represents the time delay and ϕ represents the phase shift acquired during this time delay [94]. As such, one may therefore view these as a quite general set of equations.

3.3 Simplifications and Analysis

Ignoring gain compression, spontaneous emission, and assuming a noiseless system allows us to solve the system in steady state and find a minimum and maximum allowable detuning [6] :

$$\Delta\omega_{min} = (-\kappa\frac{E_{inj}}{E_0})\sqrt{1+\alpha^2} < \Delta\omega < \kappa\frac{E_{inj}}{E_0} = \Delta\omega_{max}. \tag{3.4}$$

Similarly, the fixed phase difference between the master and slave laser, when locked, can be written in standard notation as

$$\Psi = \sin^{-1}\{\frac{\Delta\omega}{\Delta\omega_{min}}\} - \tan^{-1}(\alpha), \tag{3.5}$$

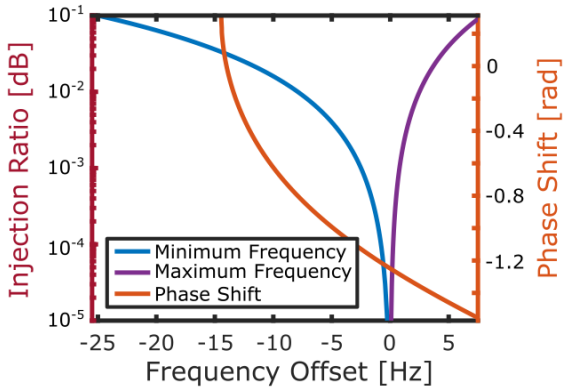

Figure 3.4: Optical injection locking simulated using the simplified set of equations. Here, the offset frequency is set to -10 GHz, and the injection ratio is varied. The asymmetry is induced by an α value of 3.

where Ψ varies between $\cot^{-1}(\alpha)$ and $\frac{-\pi}{2}$ over the locking range, and at zero detuning is equal to $-\tan^{-1}(\alpha)$.

A plot of these curves can be seen in figure 3.4, given as a function of the injection ratio, $IR = |E/E_{inj}| = \frac{\sqrt{P}}{\sqrt{P_{inj}}}$.

3.4 Control Mechanisms

OIL can be stabilized in a variety of ways [6], with the ultimate goal being a system which is robust to fluctuations on either the master or slave laser.

The simplest method of stabilization relies on the fact that when locked, the final output power of the slave laser changes minutely as a function of difference frequency, $\Delta\omega$. Therefore, by stabilizing the power at the output of the slave laser, $\Delta\omega$ can be stabilized in turn. However, because the output power is primarily governed by the slave laser, the effect is minuscule and therefore cannot be relied upon as a consistent method.

Alternatively, one can directly measure Ψ in order to stabilize the system. By assuming constant coupling, injected field power, and amplitude to phase noise conversion, equation 3.5 turns into a monotonic function of $\Delta\omega$, with bounds at the limit of injection locking. By stabilizing Ψ, one therefore stabilizes $\Delta\omega$ in turn.

Typically this is done by splitting the master laser and then modulating one arm, while leaving the other unchanged. In this case (and as seen in [Paper D]), you may lock the slave laser to the unmodulated arm and beat the slave laser output against the modulation side-band(s) of the other arm in order to recover Ψ. Alternatively, you may lock the slave laser to a modulated beam (central tone or side-bands) and, if the modulation tones are outside of the locking bandwidth, you may use the back-reflected pilot tone(s) as a reference to beat against for recovery of Ψ. In either case, the mechanism of action relies on the fact that when locked, slave lasers pick up a fixed phase shift that depends primarily on the frequency offset between the master and unperturbed slave laser operating frequency, while an unlocked tone does not.

CHAPTER 4

Frequency Combs

4.1 Combs

Optical frequency combs are a special class of highly coherent, multimode lasers which come in a variety of forms [12,13,95–101], but in all cases be described by a series of distinct, non-zero amplitude optical modes in the frequency domain which have equal spacing, and some shared offset from zero. In this case, the repetition rate of pulses is equal to the frequency spacing of optical modes, while the shared offset from $f = 0$ is equal to the carrier envelope offset (CEO) frequency. That is to say,

$$f_m = f_{\text{CEO}} + m f_{\text{rep}}. \tag{4.1}$$

In the time domain, when many mutually coherent waves are combined, a pulse is formed, as seen in figure 4.1. Mathematically, this is expressed for a frequency comb as

$$E(t) = \sum_{m=0}^{+\infty} A_m e^{i2\pi f_m t + \phi_m}. \tag{4.2}$$

An idealized, Gaussian comb can be seen in both the time and frequency domains in figure 4.2, which serves to provide an intuitive understanding of the link between the time and frequency domains via the FT. Of note, we consider a stationary pulse and define f_{CEO} as

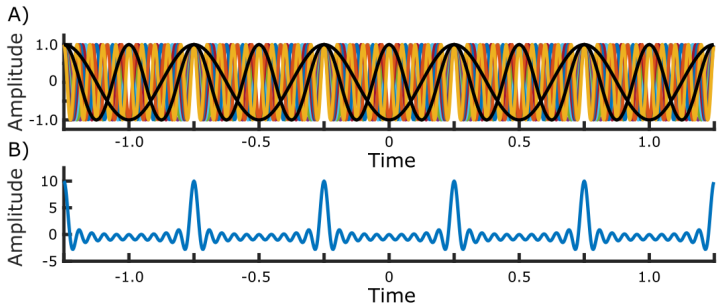

Figure 4.1: An illustration of pulse formation which occurs due to the coherent superposition of sinusoidal oscillations of different frequencies. Here, 10 cosine functions with frequencies $2\pi \cdot 5, 10, 15...50$ are coadded to generate a pulse in the time domain. By adding more and more frequency components, we are able to narrow the temporal overlap which generates pulse formation. Thus, the pulse width in time is inversely proportional to the spectral bandwidth in frequency.

$$f_{\text{CEO}} = \frac{d}{dt}\phi_{CEO}(t). \tag{4.3}$$

4.1.1 Background

Precise knowledge of an optical tone's frequency was quite difficult in the late 1990's [27, 28]. Typically, this was done using known atomic references which were useful for their reproducibility, but were hampered by the absorption profile changing as a function of temperature and pressure. Alternative solutions (in particular for frequencies not readily accessible via atomic reference), made use of long RF to optical frequency converter chains. Unfortunately, starting with a microwave reference in the low GHz and moving up to the hundreds of THz is a massively complicated process.

At it's core, this is the function of a frequency comb [13]. It serves as a link, or set of gearing, between the RF (MHz, GHz) and optical (THz) domains. Furthermore, it acts as an "optical ruler" in the sense that it lays out a set of equally spaced tick marks along a single dimension (in this case, in time/frequency as opposed to space).

The first examples of passive frequency combs were mode locked lasers using nonlinear mechanisms in the device such as a saturable ab-

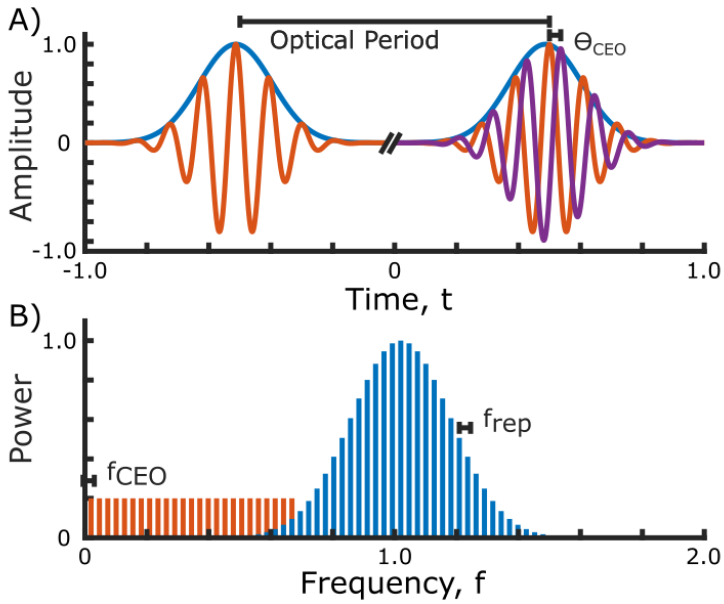

Figure 4.2: A) Two chirp free Gaussian pulses in succession, separated in the time domain by some period. Here, a copy of the first pulse (orange) is superimposed on the second (purple), to give a better indication of what is meant by the carrier envelope offset phase difference acquired between successive pulses. B) A Gaussian frequency comb in blue, with spacing between optical modes equal to the comb's repetition rate. The offset frequency shared by all optical tones is equal to the carrier envelope offset frequency, as indicated by the lowest frequency orange line which corresponds to the $m = 0$ tone. Orange tones are not real ($A_m = 0$), and are only shown to highlight the f-domain implications of the CEO frequency.

sorption mirror or the Kerr nonlinearity to provide selective gain for strong pulses and enforce a fixed phase relationship between subsequent optical modes. Alternatively, an active medium may be placed inside of the gain cavity, such as an electro- or acousto- optic modulator. The result is a set of equally spaced tones in the optical domain (set by the effective cavity round trip time in the case of passive mode locking or the driving frequency of the modulator in active mode locking). Unfortunately, the cavity itself (due to dispersion) is often not composed of equally spaced resonances, and therefore there exists some walk-off that limits the achievable spectral bandwidth - a problem which persists in photonic frequency combs to this day [102, 103].

These combs were typically locked using the "f-to-2f" method, which makes use of the fact that an octave spanning comb (often generated using nonlinear properties enabled by the high peak powers of pulsed laser systems) has access to both the $f_m = f_{CEO} + mf_{rep}$ and the $f_n = f_{CEO} + nf_{rep}$ modes, where $f_m = 2f_n$. If we frequency double the first tone, and beat it with the second, the f_{rep} terms cancel, and we're left with direct detection of the carrier envelope offset frequency, which can thereafter be stabilized. Locking with other tones (2f-3f locking, for instance) is possible using similar (albeit slightly different) math, which results in slightly higher noise [104].

4.1.2 Applications

Optical frequency combs find uses in many domains [12, 13, 105], most of which make use of the pulsed nature of light in the time domain, or the well known location of tones in the frequency domain. For instance, combs can be used to measure and transmit atomic clock signals, or can be used as optical clocks themselves (offering the best frequency stability currently available, several orders of magnitude better than traditional atomic clocks).

Combs can also be used for communications where tones sit nicely in the center of well spaced frequency bins, for the generation of arbitrary frequencies of light (as per their original purpose, and in [Papers A-B]), or be used simply as an optical reference for the calibration of spectrograms for applications such as exo-planet detection.

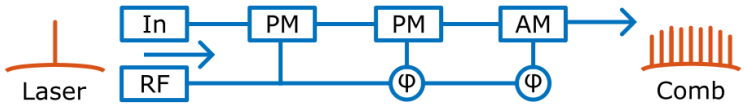

Figure 4.3: A typical EO comb setup using a low noise input laser, 2 phase modulators (PM), one amplitude modulator (AM), and an RF driving tone with phase delays between subsequent modulators to induce spectral flatness. Often, high powered RF amplifiers are used before modulation and after the phase delay (not pictured).

4.2 Electro-Optic Frequency Combs

An EO comb (figure 4.3) is one of the many varieties of frequency combs, and is created by passing a seed laser through some number of optical modulators in order to produce a series of equally spaced and cascaded modulation side-bands. Here, the comb's frequency spacing is directly determined by the modulation frequency (and thus the driving RF signal), the width of the comb is given by the strength of phase modulation, and the flatness of the spectral envelope is determined by the phase relationship between the driving field at the input of subsequent modulators.

Because the frequency line spacing (and corresponding repetition rate) is given by the RF clock which drives the modulation, ultra-high repetition rate (> 100 GHz) EO combs are difficult to produce given the lack of ultra-high repetition rate RF driving signals, amplifiers, and phase modulators. Even at moderate repetitions rates however, expensive and lossy optical modulators, powered by energy-expensive amplifiers are required. Nevertheless, EO combs are robust, easy to operate, and are well described by linear functions, as shown below. All together, this makes them of interest in both scientific and practical applications.

If we write the seed laser in terms of the classical wave equation as follows [14] :

$$A(t) = A_0 e^{i\omega_c t}, \tag{4.4}$$

where A_0 is the wave amplitude, and ω_c is the carrier frequency, then we can phase modulate the wave with some driving field to find

$$\begin{aligned} A(t) &= A_0 e^{i\omega_c t} e^{iKV_0 \sin(\omega_{\text{mod}})} \\ &= A_0 e^{i\omega_c t} e^{i\Delta\Phi}, \end{aligned} \tag{4.5}$$

where K is the phase modulation index, V_0 is the amplitude of the modulating signal, ω_{mod} is the modulation frequency, $\Delta\Phi = KV(t)$ is the phase shift due to modulation, and $V(t) = V_0 \sin(\omega_{\text{mod}} t)$.

Next, we take the FT and find that

$$\tilde{A}(\omega) = A_0 \delta(\omega - \omega_c) \int_{-\infty}^{+\infty} e^{i\Delta\Phi} e^{-i\omega t} dt, \tag{4.6}$$

where we keep in mind that $\Delta\Phi = KV(t)$ is a function of t while integrating.

We then expand the plane wave as a series of cylindrical waves (i.e. the Jacobi-Anger expansion), and write

$$\begin{aligned} \tilde{A}(\omega) &= A_0 \delta(\omega - \omega_c) \int_{-\infty}^{+\infty} \left(\sum_{n=-\infty}^{+\infty} J_n(KV_0) e^{-i(\omega - n\omega_{\text{mod}})t} \right) dt \\ &= A_0 \sum_{-\infty}^{+\infty} J_n(KV_0) \delta(\omega - n\omega_{\text{mod}} - \omega_c), \end{aligned} \tag{4.7}$$

where J_n are Bessel functions of the 1$^{\text{st}}$ kind, and act as the envelope function which defines a comb of frequencies $\omega = n\omega_{\text{mod}} + \omega_c$.

Importantly, if we introduce static some phase noise term, ϕ, which arises due to voltage fluctuations on the RF driving field, we may now write $V(t) = V_0 \sin(\omega_{\text{mod}} t + \phi)$, such that $\tilde{A}(\omega)$ becomes

$$\tilde{A}(\omega) = A_0 \sum_{-\infty}^{+\infty} J_n(KV_0) e^{in\phi} \delta(\omega - n\omega_{\text{mod}} - \omega_c), \tag{4.8}$$

and we see that the phase noise on any individual comb mode which stems from the RF oscillator that drives $V(t)$ grows linearly with absolute mode number, $|n|$, offset from the pump.

We also notice that the end result of a single phase modulator is a superposition of a large number of Bessel functions. The amplitude difference between various comb lines therefore varies considerably across the comb's bandwidth due to the complicated superposition of these Bessel functions. To compensate for this, an amplitude modulator is often placed after the phase modulator(s), in order to produce a smooth (although not necessarily a flat-top) envelope.

Figure 4.4 shows a simulated EO comb made via two phase modulators and one amplitude modulator, with a fixed phase relationship to

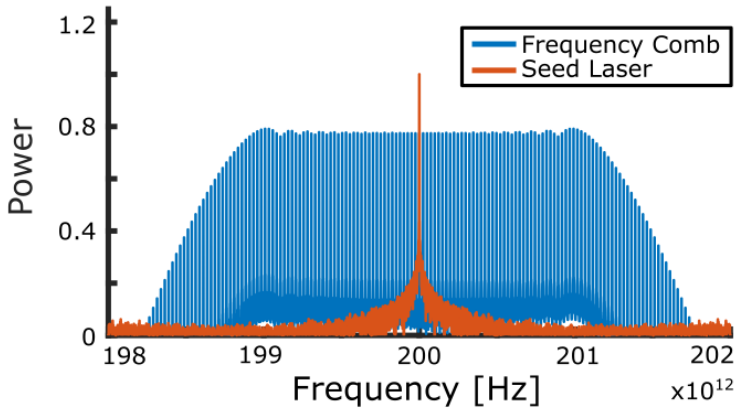

Figure 4.4: A power normalized EO comb simulated via the modulation of a noisy seed laser with an noisy RF tone. Here, two phase modulators and one amplitude modulator is used. The RF driving field is set to 24.8 GHz such that it coincides with a multiple of the simulation's sampling frequency. K is set to 3.375 V^{-1} and the amplitude modulation index is set to 0.9.

ensure maximum spectral bandwidth and a flat-top comb. The specific parameters of the simulation are such that the central frequency is set to 200 THz ($\sim$ 1500 nm), the driving RF field is set to 24.8 GHz, both the laser and modulation frequencies are given white and pink noise, and the phase modulation index, K, for both phase modulators is 3.375 V^{-1}, while the amplitude modulation index is set to 0.9.

4.3 Microresonator Frequency Combs

Photonic chip microresonator frequency combs fall under the broader category of Kerr combs [95], named for their reliance on 3rd order optical nonlinearities to produce a series of equally spaced optical tones. This is possible thanks to the build up of light in high quality factor optical cavities [16].

In general, and as seen in figure 4.5, the process can be described by a high power source traveling through a waveguide which is coupled to some high quality-factor optical resonator, where the quality factor, Q, is defined as $Q = \omega_r/\Delta\omega$, where ω_r is the angular frequency of the resonant mode in question, and $\Delta\omega$ is its FWHM bandwidth. In the limit of high Q, this definition is equivalent to 2π times the energy stored in

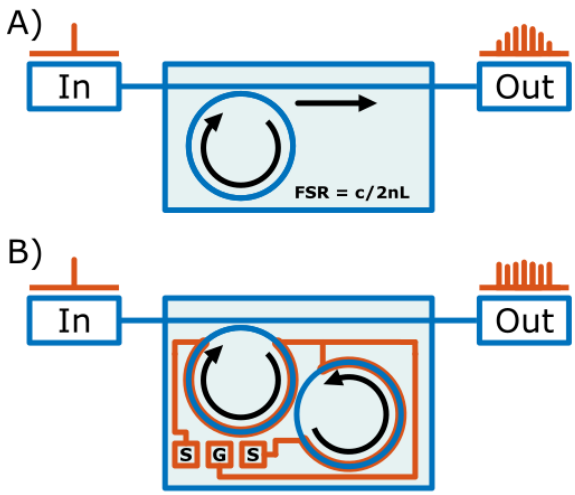

Figure 4.5: A) A high power continuous wave laser is injected into a wave guide which is coupled to a high Q-factor optical resonator. In the special case when optical gain and loss of the cavity are balanced, and nonlinear phase shift and dispersion are balanced, an optical soliton may form in the cavity, residing on top of a CW background. In this case, a highly coherent train of pulses is formed in the time domain, which corresponds to a frequency comb in the spectral domain. B) Here, the anomalous dispersion required to kick start soliton generation via modulation instability is generated locally via a tunable, avoided mode cross, using heaters on the individual, normal dispersion ring resonators.

the resonator, divided by the energy dissipated per cycle. Thus, a high quality factor cavity may allow for substantial build up of light inside the cavity.

This accumulation of electric field in the cavity is often strong enough to excite nonlinear processes (and is typically started by modulation instability in an anomalous dispersion medium [23]). Indeed, for certain values of input power relative to the waveguide's nonlinear threshold and of driving frequency relative the the cavity's natural resonance, the resulting output is a set of nonlinearly produced and equally spaced optical tones in the frequency domain (i.e. an OFC). In special cases when the cavity's gain and loss is balanced on one hand, and the nonlinear and dispersive phase shifts are balanced on the other, the output may be a stable series of soliton pulses in the time domain, sitting atop a strong continuous wave (CW) background [16].

Mathematically, the process can be thought of as a damped and driven version of the nonlinear Schrodinger equation (NLSE), which is written in dimensionless form as follows, in a form known as the dimensionless Lugiato Lefever equation (LLE) [106] :

$$\frac{\partial \Psi}{\partial T} = -(1 - i\xi_0)\Psi + \frac{i}{2}\frac{\partial^2 \Psi}{\partial \Theta^2} + i|\Psi|^2\Psi + f, \tag{4.9}$$

where $\Psi = \sqrt{\frac{2g_0}{\kappa}}A$ is the primary field,

$T = \frac{\kappa}{2}t$ represents slow time, corresponding to the wave's evolution after each roundtrip in the cavity,

$\xi_0 = \frac{2}{\kappa}(\omega_p - \omega_r)$ is the cavity detuning,

$\Theta = \sqrt{\frac{\kappa}{2D_2}}\phi$ is the dispersion normalized angular position,

$f = \sqrt{\frac{P_{\text{in}}}{P_{\text{threshold}}}}$ is the pump power relative to the threshold power,

$g_0 = \frac{\hbar\omega_0^2 c n_2}{n_g^2 V_{\text{eff}}}$ is the per photon nonlinear phase shift,

$\kappa = \kappa_{\text{intrinsic}} + \kappa_{\text{extrinsic}}$ is the inverse photon lifetime inside the cavity,

$P_{\text{threshold}} = \frac{\kappa^3}{8 g_0 \kappa_{\text{extrinsic}}}$ is the threshold power for modulation instability,

A is the field amplitude normalized to photon count,

ω_p is the pump frequency,

ω_r is the cold resonance frequency,

D_2 is the walk-off from resonance due to 2^{nd} order dispersion,

ϕ is the angular position in the cavity,

n and n_g are the regular and group indices of refraction, and

V_{eff} is the effective mode volume.

The LLE is normally solved numerically by dividing the equation into its linear ($\hat{D}$) and nonlinear ($\hat{N}$) components [107], choosing an appropriate step size in time, and solving the two components separately, in a nearly identical manner to how one would normally solve the undamped and unpumped NLSE. Of course, higher order dispersive terms and various other nonlinear effects such as the Raman effect could be considered as well [23].

Importantly, from the normalized and dimensionless LLE, we see that when given the resonator's dispersion profile, linewidth, and nonlinearity, the behavior of the system relies on only two parameters : the normalized detuning and normalized power, both of which can be controlled by acting on the driving CW laser.

When these two parameters are properly tuned relative to the given material parameters, the result is the generation of various cascaded four wave mixing (Kerr) modes in the frequency domain. Within this regime there are a large variety of still-being-explored states [108], such as the noisy, fully developed modulation instability (MI) state [109] which lacks mutual coherence between the comb lines, the multi and single soliton states (formed via an delicate balance between gain and loss on one hand, and phase shifts due to dispersion and nonlinearity on the other) [16,110], as well as more exotic states such as soliton crystals [111–113], breather solitons [114, 115], and more.

In particular, silicon nitride [116] is the only nonlinear photonic material used for Kerr soliton generation in this work, and was selected for

a variety of reasons, including its large bandgap (and therefore low loss) from 2.7 - 5 eV, its low thermo-optic coefficient around 10^{-5}, its relatively high nonlinear coefficient, its low two-photon absorption in the near infrared, the ease of dispersion tunabililty, and its compatibility with standard CMOS fabrication techniques. Still, many other material platforms are viable and are being explored at length in the field [116].

4.3.1 Normal Dispersion Coupled Cavity Combs

Typically [108], the nonlinear generation of Kerr combs depends on modulation instability which is induced by the waveguide's anomalous dispersion and which is controlled via mode field engineering [103]. However, as seen in [Papers C & D], anomalous dispersion can also be induced locally via an avoided mode crossing. In a so called "photonic molecule", two normal dispersion cavities (not able to generate modulation instability on their own due to material dispersion) are coupled together. This induces an avoided mode crossing and localized anomalous dispersion in the frequency region around the avoided mode crossing. By CW pumping in these regions of anomalous dispersion, comb generation is possible, and by using heaters attached to both resonators, the avoided mode crossing may be controlled such that the comb may be initiated at any driving frequency [18, 19]. In simulation, the auxiliary ring may be modeled simply as a change in material dispersion of the primary ring without major penalty on the validity of simulations.

CHAPTER 5

Applications and Future Outlook

In this chapter, a selection of topics related to this thesis are discussed, with a focus on the applications of optical frequency combs and optical injection locking.

5.1 Phase Sensitive Amplification

The primary motivation for producing low noise and highly tunable comb based sources in our lab is for their use in phase sensitive amplifiers [117], which are important for low noise regenerative loops, optical communications, and more.

Typically, in order to produce the idler required for phase sensitive amplification (PSA), a copier is used. Here, the pump(s) and signal are launched into some length of nonlinear medium to produce an idler wave at the required frequency. Then, the pump(s) are regenerated via amplification, their phases are fixed for maximum gain in the PSA, and the 4 waves then pass through a nonlinear medium for power conversion ('noiseless' gain). The role of a low noise highly tunable laser then, would be to replace the copier and therefore remove the need for one of the two lengths of nonlinear medium, as well potentially being used for pump regeneration at the receiver end.

A comb-based approach, where the various tones are guaranteed to be mutually coherent and equally spaced, may be used for all three waves.

A low noise pump may be used as the driving tone for comb generation, and then a signal and idler may be chosen on either side such that they are equally spaced from the center and assured to have a fixed phase relationship. Finally, optical injection locking may be used for pump recovery as a way to regenerate power lost to comb generation.

5.2 Optical Communications

In the case of optical communications, the use of ultra-low noise amplifiers is important for long haul systems where noise buildup due to amplification is often a limiting factor in system throughput [118]. A traditional optical amplifier relies on stimulated emission to produce gain, which comes with a 3 dB minimum noise floor due to ASE in the amplifier's gain medium [29].

Typically, excess out of band noise is filtered away using a BPF, which is necessarily non-resonant with the signal given that the two are unlinked. Instead, optical injection locking can be used to force an external gain cavity into resonance with the driving field, which simultaneously amplifies the desired signal while taking advantage of cavity filtration to attenuate out of band noise. This allows for the generation of a frequency selective, high gain, low noise, and narrow bandwidth amplifier to be used in optical communications, among other applications [6].

5.3 Resonant Excitation

Tunable low noise lasers are particularly interesting for their ability to excite specific and narrow resonances of a system. This could be a molecular or atomic system, such as a single vibrational mode of a particular atom or molecule, or even an optical system such as a resonant cavity.

One such application of resonant excitation may be atom trapping [119, 120] and cooling [121, 122], whereby a laser with high frequency stability manipulates some atomic material via absorption and reflection. In doing so, the photon's energy / momentum is imparted onto the atom, which can be used to lock it in place, or to effectively cool the material via a specific atomic or ionic transition.

Another common application might be the excitation of optical resonances. The typical source used in the lab for the formation in microresonator frequency combs, for example, is a low noise external cavity laser,

but could easily be replaced by a low noise tunable laser such as the one proposed here. external cavity diode laser (ECDL)s are bulky and rely on high stability of the external cavity, which makes them difficult to apply in the field. An integrated platform is compact and is necessarily more stable and thus may be more practical in out-of-lab situations [13].

5.4 Metrology and Optical Referencing

High quality lasers such as the ones discussed here are particularly useful when viewed as an absolute frequency reference, such as when calibrating various optical equipment [123], for precise measurements of distance such as in LIDAR systems, and for precision spectroscopy [124].

Metrology is a wide field with a huge range of applications, but such high fidelity measurements are particularly useful in defining standards like the length of the meter and the definition of a second. Of course, having access to a high precision frequency reference is also useful for a variety of other tasks, such as when used as a reference to which other lasers may be locked, for use as an optical clock or optical ruler, in astrophysics, etc [25].

5.5 Optical Coherence Tomography

As demonstrated in [Paper E], optical coherence tomography (OCT) is an experimental technique that aims to produce a three-dimensional image using back-scattered light. Typically, the process uses CW waves with a broad bandwidth and very low temporal coherence (or alternatively, a swept source) in order to isolate slices of a tomograph which can be reconstructed afterwards. When using a comb, however, the long coherence time and pulsed nature of the light offers an alternative method for high resolution spectral imaging [125]. Essentially, the pulse is split in two using an interferometer, with one arm used as a reference while the other is broken into various back reflections and according to frequency, will interfere with the reference arm to produce a unique pattern which may be resolved to recover an image. Broadly speaking, the device can be thought of as a massively multi-frequency interferometer. OCT has applications which are readily apparent across the field of imaging, such as the real time imaging of retinas, cardiology, oncology, dermatology, and various nondestructive testing techniques for industrial applications.

CHAPTER 6

Summary of Included Papers

Summarized here, then attached after the list of included references, are the relevant research works, Papers A - E :

Paper A
Widely tunable, low linewidth, and high power laser source using an electro-optic comb and injection-locked slave laser array
Optics Express, vol. 29, no. 11, May 2021

This paper covers work done at Chalmers, and focuses on the creation of a fixed-frequency, low noise laser source which is highly tunable. Here, a low noise seed laser is used to produce an EO frequency comb via 25 GHz cascaded modulation side bands. After comb production, a tone is picked off and used for injection locking via an array of distributed feedback (DFB) lasers. By tuning the seed laser across a frequency range greater than the RF clock's oscillation frequency, any output frequency within the comb's bandwidth is achievable at the output. This work achieves a single frequency tunable laser which has less than 400 Hz of linewidth across its full tunable range of $\sim$ 10 nm, has approximately 55 dB side-mode supression ratio (SMSR), and approximately 20 dBm of output power.

Paper B
Widely tunable narrow linewidth laser source based on photonic molecule microcombs and optical injection locking
Optics Express, vol. 30, no. 12, June 2022.

This paper covers work done at Chalmers and can be thought of as a direct follow-up work to [Paper A]. Here, the same low noise seed laser is used to produce a microresonator frequency comb in a normal dispersion photonic molecule, after which individual tones are picked off and injection locked via a single FP laser. By using a microresonator frequency comb, the free spectral range of comb lines is increased by a factor of 4 (up to 100 GHz), and by using a single FP slave laser, the complexity and footprint of the system is greatly reduced. Importantly, the use of a coupled cavity normal dispersion photonic molecule with individual heaters on each ring allows for full tunability of the final output, and provides a relatively flat-top and highly efficient comb for later injection locking. Additionally, the process addresses a huge number of size, weight, and power (SWaP) concerns compared to traditional, bulk EO-combs. The resulting output does incur some penalty in phase/frequency noise and in final output power when compared to the result of [Paper A] , but is significantly more tunable (notably, across the full C-Band of operation).

Paper C
Thermorefractive noise reduction of photonic molecule frequency combs using an all-optical servo loop
Optics Express, vol. 31, no. 21, October 2023.

This paper covers work done in collaboration with DTU and at NKT photonics as part of an industry exchange during my PhD at Chalmers, and can be thought of as a direct follow-up work to [Paper B]. In the previous paper, thermorefractive noise was identified as the main limiting factor contributing to phase noise at the system output, and as the main driving source for phase noise growth as a function of comb mode index. These thermal effects are present in all systems, but can be mitigated in optical microcavities by placing a 'cooling' or 'servo' laser on the blue side of a compatible optical resonance, such that it may passively compensate for temperature fluctuations. This process, however, has been traditionally limited by the initiation of modulation

instability in anomalous dispersion media as power on the secondary laser increases. Due to the way in which normal dispersion photonic molecules produce a comb, however, dispersion is only anomalous near the pump frequency, and therefore, cooling may be achieved past the typical nonlinear power limit imposed by anomalous dispersion in a traditional microcomb.

Paper D
Pre-amplified optical injection locking at low input powers
submitted to *Optics Express*.

This paper covers work done at Chalmers, and is focused on the limits of optical injection locking. We find that when the injection ratio is very low (such that the locking bandwidth is narrow) and when noise on the injected signal is high, temporary fluctuations may be able to momentarily unlock the system. This results in a phase slip in the difference between master and slave laser, which corresponds to a spike in the phase noise PSD. The process is studied in simulations and, experimentally, we demonstrate the recovery of tones at powers as low as -80 dBm (-70 dBm for phase slip free operation), producing a frequency copy of the input CW signal at the slave laser output of approximately 20 dBm. Here, a PID loop is used to lock Ψ by feeding back on the slave laser.

Paper E
Soliton microcomb based spectral domain optical coherence tomography
Nature Communications, 12:427, 2021.

This paper covers work done at EPFL, and focuses on the application of microresonator frequency combs to optical coherence tomography - comparing the soliton and MI states of an anomalous dispersion microresonator frequency comb to a traditional OCT source such as the superluminescent diode. In particular, we are interested in the relative intensity noise of both the single soliton and chaotic MI states, as well as the degree of intensity cross correlation between various comb lines. Importantly, common-mode noise will not degrade the ultimate dynamic range of the imaging system, and as such - the soliton state offers several advantages. That being said, the discretization of

the frequency components does lead to periodicity in the image which may introduce additional complexity.

References

[1] A. E. Siegman, "Lasers," *Mill Valley, CA*, vol. 37, no. 208, p. 169, 1986.

[2] A. J. Gross and T. R. Herrmann, "History of lasers," *World Journal of Urology*, vol. 25, no. 3, pp. 217–220, 2007.

[3] J. Ohtsubo and J. Ohtsubo, *Semiconductor lasers and theory*. Springer, 2017.

[4] W. W. Chow, S. W. Koch, and M. I. Sargent, *Semiconductor-laser physics*. Springer Science & Business Media, 2012.

[5] R. Dupuis, "An introduction to the development of the semiconductor laser," *IEEE Journal of Quantum Electronics*, vol. 23, no. 6, pp. 651–657, 1987.

[6] Z. Liu and R. Slavík, "Optical injection locking: From principle to applications," *Journal of Lightwave Technology*, vol. 38, no. 1, pp. 43–59, 2020.

[7] R. Lang, "Injection locking properties of a semiconductor laser," *IEEE Journal of Quantum Electronics*, vol. 18, no. 6, pp. 976–983, 1982.

[8] F. Mogensen, H. Olesen, and G. Jacobsen, "Locking conditions and stability properties for a semiconductor laser with external light injection," *IEEE Journal of Quantum Electronics*, vol. 21, no. 7, pp. 784–793, 1985.

[9] R. Hui, A. D'Ottavi, A. Mecozzi, and P. Spano, "Injection locking in distributed feedback semiconductor lasers," *IEEE Journal of Quantum Electronics*, vol. 27, no. 6, pp. 1688–1695, 1991.

[10] W. Yang, P. Guo, D. Parekh, and C. J. Chang-Hasnain, "Reflection-mode optical injection locking," *Optics Express*, vol. 18, no. 20, pp. 20 887–20 893, 2010.

[11] G. Van Tartwijk and D. Lenstra, "Semiconductor lasers with optical injection and feedback," *Quantum and Semiclassical Optics: Journal of the European Optical Society Part B*, vol. 7, no. 2, p. 87, 1995.

[12] T. Fortier and E. Baumann, "20 years of developments in optical frequency comb technology and applications," *Communications Physics*, vol. 2, no. 1, pp. 1–16, 2019.

[13] S. A. Diddams, K. Vahala, and T. Udem, "Optical frequency combs: coherently uniting the electromagnetic spectrum," *Science*, vol. 369, no. 6501, 2020.

[14] A. Parriaux, K. Hammani, and G. Millot, "Electro-optic frequency combs," *Advances in Optics and Photonics*, vol. 12, no. 1, pp. 223–287, 2020.

[15] R. Zhuang, K. Ni, G. Wu, T. Hao, L. Lu, Y. Li, and Q. Zhou, "Electro-optic frequency combs: Theory, characteristics, and applications," *Laser & Photonics Reviews*, p. 2200353, 2023.

[16] T. J. Kippenberg, A. L. Gaeta, M. Lipson, and M. L. Gorodetsky, "Dissipative kerr solitons in optical microresonators," *Science*, vol. 361, no. 6402, p. eaan8083, 2018.

[17] A. Pasquazi, M. Peccianti, L. Razzari, D. J. Moss, S. Coen, M. Erkintalo, Y. K. Chembo, T. Hansson, S. Wabnitz, P. DelHaye *et al.*, "Micro-combs: A novel generation of optical sources," *Physics Reports*, vol. 729, pp. 1–81, 2018.

[18] X. Xue, Y. Xuan, P.-H. Wang, Y. Liu, D. E. Leaird, M. Qi, and A. M. Weiner, "Normal-dispersion microcombs enabled by controllable mode interactions," *Laser & Photonics Reviews*, vol. 9, no. 4, pp. L23–L28, 2015.

[19] Ó. B. Helgason, F. R. Arteaga-Sierra, Z. Ye, K. Twayana, P. A. Andrekson, M. Karlsson, J. Schröder, and V. Torres-Company, "Dissipative solitons in photonic molecules," *Nature Photonics*, vol. 15, no. 4, pp. 305–310, 2021.

[20] A. Chodos and J. Ouellette, "This month in physics history: December 1958: invention of the laser," *APS News*, vol. 12, no. 11, 2003.

[21] J. Hecht, "Short history of laser development," *Optical Engineering*, vol. 49, no. 9, pp. 091 002–091 002, 2010.

[22] G. P. Agrawal, "Nonlinear fiber optics," in *Nonlinear Science at the Dawn of the 21st Century*. Springer, 2000, pp. 195–211.

[23] R. W. Boyd, A. L. Gaeta, and E. Giese, "Nonlinear optics," in *Springer Handbook of Atomic, Molecular, and Optical Physics*. Springer, 2008, pp. 1097–1110.

[24] J. Stenger, H. Schnatz, C. Tamm, and H. R. Telle, "Ultraprecise measurement of optical frequency ratios," *Physical Review Letters*, vol. 88, no. 7, p. 073601, 2002.

[25] T. Udem, R. Holzwarth, and T. W. Hänsch, "Optical frequency metrology," *Nature*, vol. 416, no. 6877, pp. 233–237, 2002.

[26] L. Hollberg, C. W. Oates, E. A. Curtis, E. N. Ivanov, S. A. Diddams, T. Udem, H. G. Robinson, J. C. Bergquist, R. J. Rafac, W. M. Itano *et al.*, "Optical frequency standards and measurements," *IEEE Journal of Quantum Electronics*, vol. 37, no. 12, pp. 1502–1513, 2001.

[27] J. L. Hall, "Nobel lecture: Defining and measuring optical frequencies," *Reviews of Modern Physics*, vol. 78, no. 4, p. 1279, 2006.

[28] T. W. Hänsch, "Nobel lecture: Passion for precision," *Reviews of Modern Physics*, vol. 78, no. 4, p. 1297, 2006.

[29] G. P. Agrawal, *Fiber-optic communication systems*. John Wiley & Sons, 2012, vol. 222.

[30] E. Agrell, M. Karlsson, A. Chraplyvy, D. J. Richardson, P. M. Krummrich, P. Winzer, K. Roberts, J. K. Fischer, S. J. Savory,

B. J. Eggleton *et al.*, "Roadmap of optical communications," *Journal of Optics*, vol. 18, no. 6, p. 063002, 2016.

[31] G. P. Agrawal, "Optical communication: its history and recent progress," *Optics in Our Time*, pp. 177–199, 2016.

[32] E. D. Kaplan and C. Hegarty, *Understanding GPS/GNSS: principles and applications*. Artech house, 2017.

[33] U. Wandinger, "Introduction to lidar," in *LIDAR: range-resolved optical remote sensing of the atmosphere*. Springer, 2005, pp. 1–18.

[34] B. P. Abbott, R. Abbott, T. Abbott, M. Abernathy, F. Acernese, K. Ackley, C. Adams, T. Adams, P. Addesso, R. Adhikari *et al.*, "Observation of gravitational waves from a binary black hole merger," *Physical Review Letters*, vol. 116, no. 6, p. 061102, 2016.

[35] T. Wilken, C. Lovis, A. Manescau, T. Steinmetz, L. Pasquini, G. Lo Curto, T. W. Hänsch, R. Holzwarth, and T. Udem, "High-precision calibration of spectrographs," *Monthly Notices of the Royal Astronomical Society: Letters*, vol. 405, no. 1, pp. L16–L20, 2010.

[36] M. Adams, "Rate equations and transient phenomena in semiconductor lasers," *Opto-Electronics*, vol. 5, pp. 201–215, 1973.

[37] G. Bjork and Y. Yamamoto, "Analysis of semiconductor microcavity lasers using rate equations," *IEEE Journal of Quantum Electronics*, vol. 27, no. 11, pp. 2386–2396, 1991.

[38] D. Marcuse, "Classical derivation of the laser rate equation," *IEEE Journal of Quantum Electronics*, vol. 19, no. 8, pp. 1228–1231, 1983.

[39] J.-F. Mercier and J. Moloney, "Derivation of semiconductor laser mean-field and Swift-Hohenberg equations," *Physical Review E*, vol. 66, no. 3, p. 036221, 2002.

[40] J. C. Cartledge and R. Srinivasan, "Extraction of DFB laser rate equation parameters for system simulation purposes," *Journal of Lightwave Technology*, vol. 15, no. 5, pp. 852–860, 1997.

[41] A. L. Schawlow and C. H. Townes, "Infrared and optical masers," *Phys. Rev.*, vol. 112, pp. 1940–1949, Dec 1958.

[42] M. Yamada, "Theory of mode competition noise in semiconductor injection lasers," *IEEE Journal of Quantum Electronics*, vol. 22, no. 7, pp. 1052–1059, 1986.

[43] J. Dellunde, M. Torrent, J. Sancho, and M. San Miguel, "Frequency dynamics of gain-switched injection-locked semiconductor lasers," *IEEE Journal of Quantum Electronics*, vol. 33, no. 9, pp. 1537–1542, 1997.

[44] S. P. Ó Dúill, P. M. Anandarajah, R. Zhou, and L. P. Barry, "Numerical investigation into the injection-locking phenomena of gain switched lasers for optical frequency comb generation," *Applied Physics Letters*, vol. 106, no. 21, 2015.

[45] J. C. Butcher, "A history of Runge-Kutta methods," *Applied Numerical Mathematics*, vol. 20, no. 3, pp. 247–260, 1996.

[46] I. Joindot, "Measurements of relative intensity noise (RIN) in semiconductor lasers," *Journal de Physique III*, vol. 2, no. 9, pp. 1591–1603, 1992.

[47] J. Peng, H. Yu, J. Liu, Y. Cao, Z. Zhang, and L. Sun, "Principles, measurements and suppressions of semiconductor laser noise, a review," *IEEE Journal of Quantum Electronics*, vol. 57, no. 5, pp. 1–15, 2021.

[48] X. Cheng, W. Pan, X. Zeng, J. Dong, S. Cui, and Y. Feng, "Relative intensity noise comparison of fiber laser and amplified spontaneous emission sources," *Optical Fiber Technology*, vol. 54, p. 102119, 2020.

[49] C. W. Nelson, A. Hati, and D. A. Howe, "Relative intensity noise suppression for RF photonic links," *IEEE Photonics Technology Letters*, vol. 20, no. 18, pp. 1542–1544, 2008.

[50] M. Huber, W. Schweinberger, F. Stutzki, J. Limpert, I. Pupeza, and O. Pronin, "Active intensity noise suppression for a broadband mid-infrared laser source," *Optics Express*, vol. 25, no. 19, pp. 22 499–22 509, 2017.

[51] B. E. Saleh and M. C. Teich, *Fundamentals of photonics*. John Wiley & Sons, 2019.

[52] S. B. Lowen and M. C. Teich, "Power law shot noise," *IEEE Transactions on information theory*, vol. 36, no. 6, pp. 1302–1318, 1990.

[53] A. Van Der Ziel, "Noise in solid-state devices and lasers," *Proceedings of the IEEE*, vol. 58, no. 8, pp. 1178–1206, 1970.

[54] M. Lax, "Theory of laser noise," in *Laser Noise*, vol. 1376. SPIE, 1991, pp. 2–20.

[55] E. Rubiola and V. Giordano, "Phase noise metrology," in *Noise, Oscillators and Algebraic Randomness: From Noise in Communication Systems of Number Theory Lectures of a School Held in Chapelle des Bois, France, April 5–10, 1999*. Springer, 2000, pp. 189–215.

[56] H. Wenzel, M. Kantner, M. Radziunas, and U. Bandelow, "Semiconductor laser linewidth theory revisited," *Applied Sciences*, vol. 11, no. 13, p. 6004, 2021.

[57] G. M. Stéphan, T. Tam, S. Blin, P. Besnard, and M. Têtu, "Laser line shape and spectral density of frequency noise," *Physical Review A*, vol. 71, no. 4, p. 043809, 2005.

[58] C. Henry, "Theory of the linewidth of semiconductor lasers," *IEEE Journal of Quantum Electronics*, vol. 18, no. 2, pp. 259–264, 1982.

[59] P. Goldberg, P. W. Milonni, and B. Sundaram, "Theory of the fundamental laser linewidth," *Physical Review A*, vol. 44, no. 3, p. 1969, 1991.

[60] M. Ohtsu, K. Nakagawa, M. Kourogi, and W. Wang, "Frequency control of semiconductor lasers," *Journal of Applied Physics*, vol. 73, no. 12, pp. R1–R17, 1993.

[61] M. A. Tran, D. Huang, and J. E. Bowers, "Tutorial on narrow linewidth tunable semiconductor lasers using Si/III-V heterogeneous integration," *APL Photonics*, vol. 4, no. 11, p. 111101, 2019.

[62] G. Di Domenico, S. Schilt, and P. Thomann, "Simple approach to the relation between laser frequency noise and laser line shape," *Applied Optics*, vol. 49, no. 25, pp. 4801–4807, 2010.

[63] C. H. Henry and R. F. Kazarinov, "Quantum noise in photonics," *Reviews of Modern Physics*, vol. 68, no. 3, p. 801, 1996.

[64] B. Mulgrew, P. Grant, and J. Thompson, *Digital signal processing: concepts and applications*. Bloomsbury Publishing, 2002.

[65] S. Camatel and V. Ferrero, "Narrow linewidth CW laser phase noise characterization methods for coherent transmission system applications," *Journal of Lightwave Technology*, vol. 26, no. 17, pp. 3048–3055, 2008.

[66] N. Satyan, J. B. Sendowski, A. Vasilyev, G. A. Rakuljic, and A. Yariv, "Phase noise reduction of a semiconductor laser in a composite optical phase-locked loop," *Optical Engineering*, vol. 49, no. 12, p. 124301, 2010.

[67] D. Arsenijević, M. Kleinert, and D. Bimberg, "Phase noise and jitter reduction by optical feedback on passively mode-locked quantum-dot lasers," *Applied Physics Letters*, vol. 103, no. 23, p. 231101, 2013.

[68] C. McNeilage, E. Ivanov, P. Stockwell, and J. Searls, "Review of feedback and feedforward noise reduction techniques," in *Proceedings of the 1998 IEEE International Frequency Control Symposium (Cat. No. 98CH36165)*. IEEE, 1998, pp. 146–155.

[69] F. Aflatouni, M. Bagheri, and H. Hashemi, "Design methodology and architectures to reduce the semiconductor laser phase noise using electrical feedforward schemes," *IEEE Transactions on Microwave Theory and Techniques*, vol. 58, no. 11, pp. 3290–3303, 2010.

[70] K. Shin and J. Hammond, *Fundamentals of signal processing for sound and vibration engineers*. John Wiley & Sons, 2008.

[71] K. Ogawa, "Considerations for optical receiver design," *IEEE Journal on Selected Areas in Communications*, vol. 1, no. 3, pp. 524–532, 1983.

[72] X. Xie, R. Bouchand, D. Nicolodi, M. Lours, C. Alexandre, and Y. Le Coq, "Phase noise characterization of sub-Hertz linewidth lasers via digital cross correlation," *Optics Letters*, vol. 42, no. 7, pp. 1217–1220, 2017.

[73] L. Richter, H. Mandelberg, M. Kruger, and P. McGrath, "Linewidth determination from self-heterodyne measurements with subcoherence delay times," *IEEE Journal of Quantum Electronics*, vol. 22, no. 11, pp. 2070–2074, 1986.

[74] O. Llopis, P.-H. Merrer, H. Brahimi, K. Saleh, and P. Lacroix, "Phase noise measurement of a narrow linewidth CW laser using delay line approaches," *Optics Letters*, vol. 36, no. 14, pp. 2713–2715, 2011.

[75] M. Xue and J. Zhao, "Laser linewidth measurement based on long and short delay fiber combination," *Optics Express*, vol. 29, no. 17, pp. 27 118–27 126, 2021.

[76] S. Huang, T. Zhu, Z. Cao, M. Liu, M. Deng, J. Liu, and X. Li, "Laser linewidth measurement based on amplitude difference comparison of coherent envelope," *IEEE Photonics Technology Letters*, vol. 28, no. 7, pp. 759–762, 2016.

[77] Z. Wang, C. Ke, Y. Zhong, C. Xing, H. Wang, K. Yang, S. Cui, and D. Liu, "Ultra-narrow-linewidth measurement utilizing dual-parameter acquisition through a partially coherent light interference," *Optics Express*, vol. 28, no. 6, pp. 8484–8493, 2020.

[78] T. L. Koch and J. E. Bowers, "Nature of wavelength chirping in directly modulated semiconductor lasers," *Electronics letters*, vol. 20, no. 25, pp. 1038–1040, 1984.

[79] X. Li and W.-P. Huang, "Simulation of DFB semiconductor lasers incorporating thermal effects," *IEEE Journal of Quantum Electronics*, vol. 31, no. 10, pp. 1848–1855, 1995.

[80] G. Sinatkas, T. Christopoulos, O. Tsilipakos, and E. E. Kriezis, "Electro-optic modulation in integrated photonics," *Journal of Applied Physics*, vol. 130, no. 1, 2021.

[81] S. Bennett, "Nicholas Minorsky and the automatic steering of ships," *IEEE Control Systems Magazine*, vol. 4, no. 4, pp. 10–15, 1984.

[82] J. Youney, "A comparison and evaluation of common PID tuning methods," University of Central Florida, Tech. Rep., 2007.

[83] O. A. Somefun, K. Akingbade, and F. Dahunsi, "The dilemma of PID tuning," *Annual Reviews in Control*, vol. 52, pp. 65–74, 2021.

[84] M. J. Connelly, *Semiconductor optical amplifiers*. Springer Science & Business Media, 2007.

[85] M. Wasfi, "Optical fiber amplifiers-review," *International Journal of Communication Networks and Information Security (IJCNIS)*, vol. 1, no. 1, pp. 42–47, 2009.

[86] B. Razavi, "A study of injection locking and pulling in oscillators," *IEEE Journal of Solid-state Circuits*, vol. 39, no. 9, pp. 1415–1424, 2004.

[87] L. Paciorek, "Injection locking of oscillators," *Proceedings of the IEEE*, vol. 53, no. 11, pp. 1723–1727, 1965.

[88] X. J. Meng, T. Chau, and M. C. Wu, "Improved intrinsic dynamic distortions in directly modulated semiconductor lasers by optical injection locking," *IEEE Transactions on Microwave Theory and Techniques*, vol. 47, no. 7, pp. 1172–1176, 1999.

[89] E. K. Lau, H.-K. Sung, and M. C. Wu, "Frequency response enhancement of optical injection-locked lasers," *IEEE Journal of Quantum Electronics*, vol. 44, no. 1, pp. 90–99, 2007.

[90] I. Petitbon, P. Gallion, G. Debarge, and C. Chabran, "Locking bandwidth and relaxation oscillations of an injection-locked semiconductor laser," *IEEE Journal of Quantum Electronics*, vol. 24, no. 2, pp. 148–154, 1988.

[91] X. Jin and S.-L. Chuang, "Relative intensity noise characteristics of injection-locked semiconductor lasers," *Applied Physics Letters*, vol. 77, no. 9, pp. 1250–1252, 2000.

[92] E. K. Lau, L. J. Wong, and M. C. Wu, "Enhanced modulation characteristics of optical injection-locked lasers: A tutorial," *IEEE Journal of Selected Topics in Quantum Electronics*, vol. 15, no. 3, pp. 618–633, 2009.

[93] H. Rong-Qing and T. Shang-Ping, "Improved rate equations for external cavity semiconductor lasers," *IEEE Journal of Quantum Electronics*, vol. 25, no. 6, pp. 1580–1584, 1989.

[94] B. Tromborg and J. Mork, "Nonlinear injection locking dynamics and the onset of coherence collapse in external cavity lasers," *IEEE Journal of Quantum Electronics*, vol. 26, no. 4, pp. 642–654, 1990.

[95] Y. K. Chembo, "Kerr optical frequency combs: theory, applications and perspectives," *Nanophotonics*, vol. 5, no. 2, pp. 214–230, 2016.

[96] J. Li, Y. Qu, R. Yu, and Y. Wu, "Generation and control of optical frequency combs using cavity electromagnetically induced transparency," *Physical Review A*, vol. 97, no. 2, p. 023826, 2018.

[97] T. Tanabe, S. Fujii, and R. Suzuki, "Review on microresonator frequency combs," *Japanese Journal of Applied Physics*, vol. 58, no. SJ, p. SJ0801, 2019.

[98] T. Udem and F. Riehle, "Frequency combs applications and optical frequency standards," *La Rivista del Nuovo Cimento*, vol. 30, no. 12, pp. 563–606, 2007.

[99] T. Udem, R. Holzwarth, and T. Hänsch, "Femtosecond optical frequency combs," *The European Physical Journal Special Topics*, vol. 172, no. 1, pp. 69–79, 2009.

[100] M. Zajnulina, J. C. Boggio, M. Böhm, A. A. Rieznik, T. Fremberg, R. Haynes, and M. Roth, "Generation of optical frequency combs via four-wave mixing processes for low-and medium-resolution astronomy," *Applied Physics B*, vol. 120, no. 1, pp. 171–184, 2015.

[101] A. Rueda, F. Sedlmeir, M. Kumari, G. Leuchs, and H. G. Schwefel, "Resonant electro-optic frequency comb," *Nature*, vol. 568, no. 7752, pp. 378–381, 2019.

[102] L. Chang, S. Liu, and J. E. Bowers, "Integrated optical frequency comb technologies," *Nature Photonics*, vol. 16, no. 2, pp. 95–108, 2022.

[103] J. Riemensberger, K. Hartinger, T. Herr, V. Brasch, R. Holzwarth, and T. J. Kippenberg, "Dispersion engineering of thick high-Q silicon nitride ring-resonators via atomic layer deposition," *Optics Express*, vol. 20, no. 25, pp. 27 661–27 669, 2012.

[104] D. J. Jones, S. A. Diddams, J. K. Ranka, A. Stentz, R. S. Windeler, J. L. Hall, and S. T. Cundiff, "Carrier-envelope phase control of

femtosecond mode-locked lasers and direct optical frequency synthesis," *Science*, vol. 288, no. 5466, pp. 635–639, 2000.

[105] S. A. Diddams, "The evolving optical frequency comb," *JOSA B*, vol. 27, no. 11, pp. B51–B62, 2010.

[106] E. G. A. Lucas, "Physics of dissipative Kerr solitons in optical microresonators and application to frequency synthesis," EPFL, Tech. Rep., 2019.

[107] L. Lugiato, F. Prati, M. Gorodetsky, and T. Kippenberg, "From the lugiato–lefever equation to microresonator-based soliton Kerr frequency combs," *Philosophical Transactions of the Royal Society A: Mathematical, Physical and Engineering Sciences*, vol. 376, no. 2135, p. 20180113, 2018.

[108] T. Herr, K. Hartinger, J. Riemensberger, C. Wang, E. Gavartin, R. Holzwarth, M. Gorodetsky, and T. Kippenberg, "Universal formation dynamics and noise of Kerr-frequency combs in microresonators," *Nature Photonics*, vol. 6, no. 7, pp. 480–487, 2012.

[109] A. Coillet and Y. K. Chembo, "Routes to spatiotemporal chaos in Kerr optical frequency combs," *Chaos: An Interdisciplinary Journal of Nonlinear Science*, vol. 24, no. 1, p. 013113, 2014.

[110] Z. Kang, F. Li, J. Yuan, K. Nakkeeran, J. N. Kutz, Q. Wu, C. Yu, and P. Wai, "Deterministic generation of single soliton Kerr frequency comb in microresonators by a single shot pulsed trigger," *Optics Express*, vol. 26, no. 14, pp. 18 563–18 577, 2018.

[111] D. C. Cole, E. S. Lamb, P. Del'Haye, S. A. Diddams, and S. B. Papp, "Soliton crystals in Kerr resonators," *Nature Photonics*, vol. 11, no. 10, pp. 671–676, 2017.

[112] M. Karpov, M. H. Pfeiffer, H. Guo, W. Weng, J. Liu, and T. J. Kippenberg, "Dynamics of soliton crystals in optical microresonators," *Nature Physics*, vol. 15, no. 10, pp. 1071–1077, 2019.

[113] Y. He, J. Ling, M. Li, and Q. Lin, "Perfect soliton crystals on demand," *Laser & Photonics Reviews*, vol. 14, no. 8, p. 1900339, 2020.

[114] E. Lucas, M. Karpov, H. Guo, M. Gorodetsky, and T. J. Kippenberg, "Breathing dissipative solitons in optical microresonators," *Nature Communications*, vol. 8, no. 1, pp. 1–11, 2017.

[115] H. Guo, E. Lucas, M. H. Pfeiffer, M. Karpov, M. Anderson, J. Liu, M. Geiselmann, J. D. Jost, and T. J. Kippenberg, "Intermode breather solitons in optical microresonators," *Physical Review X*, vol. 7, no. 4, p. 041055, 2017.

[116] A. Kovach, D. Chen, J. He, H. Choi, A. H. Dogan, M. Ghasemkhani, H. Taheri, and A. M. Armani, "Emerging material systems for integrated optical Kerr frequency combs," *Advances in Optics and Photonics*, vol. 12, no. 1, pp. 135–222, 2020.

[117] P. A. Andrekson and M. Karlsson, "Fiber-based phase-sensitive optical amplifiers and their applications," *Advances in Optics and Photonics*, vol. 12, no. 2, pp. 367–428, 2020.

[118] A. Bononi, J.-C. Antona, and P. Serena, "The generalized Droop model for optical long-haul transmission systems." in *ECOC*, 2020.

[119] C. Bradac, "Nanoscale optical trapping: a review," *Advanced Optical Materials*, vol. 6, no. 12, p. 1800005, 2018.

[120] M. Tomza, K. Jachymski, R. Gerritsma, A. Negretti, T. Calarco, Z. Idziaszek, and P. S. Julienne, "Cold hybrid ion-atom systems," *Reviews of Modern Physics*, vol. 91, no. 3, p. 035001, 2019.

[121] B. Zhao, M. Hu, X. Ao, N. Chen, and G. Pei, "Radiative cooling: A review of fundamentals, materials, applications, and prospects," *Applied Energy*, vol. 236, pp. 489–513, 2019.

[122] L. Anderegg, B. L. Augenbraun, Y. Bao, S. Burchesky, L. W. Cheuk, W. Ketterle, and J. M. Doyle, "Laser cooling of optically trapped molecules," *Nature Physics*, vol. 14, no. 9, pp. 890–893, 2018.

[123] E. Goetz and R. Savage, "Calibration of the LIGO displacement actuators via laser frequency modulation," *Classical and Quantum Gravity*, vol. 27, no. 21, p. 215001, 2010.

[124] W. Majewski, "A tunable, single frequency UV source for high resolution spectroscopy in the 293–330 nm range," *Optics Communications*, vol. 45, no. 3, pp. 201–206, 1983.

[125] J. M. Schmitt, "Optical coherence tomography (OCT): a review," *IEEE Journal of Selected Topics in Quantum Electronics*, vol. 5, no. 4, pp. 1205–1215, 1999.

Included papers A–E

Paper A

"Widely tunable, low linewidth, and high power laser source using an electro-optic comb and injection-locked slave laser array"

J. Connor Skehan, Corentin Naveau, Jochen Schröder, and Peter Andrekson

Optics Express, vol. 29, no. 11, May 2022

Paper B

"Widely tunable narrow linewidth laser source based on photonic molecule microcombs and optical injection locking"
J. Connor Skehan, Óskar Helgason, Jochen Schröder, and Peter Andrekson
Optics Express, vol. 30, no. 12, June 2022.

Paper C

"Thermorefractive noise reduction of photonic molecule frequency combs using an all-optical servo loop"
J. Connor Skehan, Anamika Nair Karunakaran, Poul Varming, Óskar Helgason, Patrick Montague, Jochen Schröder, Minhao Pu, Kresten Yvind, Peter Andrekson
Optics Express, vol. 31, no. 21, October 2023.

Paper D

"Pre-amplified optical injection locking at low input powers"
J. Connor Skehan, Magnus Karlsson, and Peter Andrekson
submitted to *Optics Express*.

Paper E

"Soliton microcomb based spectral domain optical coherence tomography"
Paul J. Marchand, Johann Riemensberger, **J. Connor Skehan**, Jia-Jung Ho, Martin H. P. Pfeiffer, Junqiu Liu, Christoph Hauger, Theo Lasser, Tobias J. Kippenberg
Nature Communications, 12:427, 2021.